

MASTER'S THESIS

---

# The Influence of Tides on Anisotropic Eddy Diffusivities in the Labrador Sea Using a Lagrangian Framework

---

*Author:*  
Tycho Bovenschen

*Supervisors:*  
Dr. Erik van Sebille  
Prof. dr. Leo Maas  
Daan Reijnders MSc

July 26, 2021



**Universiteit Utrecht**

Institute for Marine and Atmospheric research Utrecht  
Department of Physics  
Utrecht University

## Abstract

In ocean models the evolution of a tracer is generally assumed to be caused by two different processes; advection by the mean flow and diffusion. Diffusion parameterizes all non-resolved processes and the rate of diffusion is given by the diffusivity. This diffusivity is often assumed to be isotropic or even constant, however due to different processes, it can be greatly enhanced or suppressed in certain directions, giving rise to anisotropies. We investigated the influence of the tides on these diffusivities in the horizontal plane. Using a simple kinematic model we studied the interaction of different components of the velocity fields and how this affects the effective diffusivity. These concepts were then applied to a more realistic study in the Labrador Sea where we calculated diffusivities from Lagrangian model simulations, with and without tides, as well as from GPS drifter observations. We showed that the interaction of the tides with eddies or a shear flow can have a large influence on the diffusivities, greatly enhancing it in the direction of the tidal excursion. This effect depends on the length and velocity scales of the eddies and the tides, as well as on the angle the tides make with the eddy field. A shear flow perpendicular to the tidal flow can reduce this effect of the tides, suppressing the mixing in the cross-flow direction. The Lagrangian model simulations in the Labrador Sea indeed showed largely increased and anisotropic diffusivities due to the tides. The same effect of the tides was however not observed in the diffusivities calculated from drifter observations, possibly due to a lack of data in areas with large tidal currents. Furthermore, the diffusivities from the observational data were in general larger, mainly in the areas with large mean currents. This might be the effect of shear dispersion and subgrid-scale processes. In general this research shows that the tides can have a large influence on the diffusivity when the tidal currents are strong enough. This effect is however hard to observe from drifter data, since these areas are often not very well sampled. This implies that ocean models would perform better in tidal regions and in regions with high shear gradients if anisotropic diffusivities were included.

# 1 Acknowledgements

Firstly I want to thank my supervisors Erik, Leo and Daan for helping me throughout the process of writing my thesis. I realize that I have been lucky to have three supervisors that I saw every week. Even though we have mainly seen each other via teams you were really engaged and helpful and with your different backgrounds you really complemented each other. Erik, you always had so many ideas and input of what I could do, giving me a direction when I did not know where to go. Leo, with your background in tides and math you often made me think about my results in a different way, also linking it to existing literature. And Daan, thanks for always being available when I had extra questions and for patiently explaining your views and knowledge about diffusion.

Furthermore I want to thank the rest of the Parcels group for making me feel very welcome and part of the team. Especially I am also grateful to Reint, who helped me a lot with working with Gemini and Parcels and Steffie for helping with my presentation.

In addition, I want to thank Sophie and Ina for drinking all the coffees together at the University and for having many interesting and useful discussions, making my working days much more fun. Menno and Tjeerd, thanks for taking the time to check my thesis and lastly, thanks Rens and Lisette that you were always there to cheer me up when I had a hard time.

## 2 Table of acronyms

CMEMS	Copernicus Marine Environment Monitoring Service
SMOC	Surface and Merged Ocean Currents
NOAA	National Oceanic and Atmospheric Administration (from the USA)
ITS	Integral time scale
WGC	West Greenland Current
FES	Finite element solution

Table 1: Table of acronyms

# Contents

<b>1</b>	<b>Acknowledgements</b>	<b>2</b>
<b>2</b>	<b>Table of acronyms</b>	<b>3</b>
<b>3</b>	<b>Introduction</b>	<b>5</b>
<b>4</b>	<b>Theory</b>	<b>7</b>
4.1	Diffusion: Eulerian framework . . . . .	7
4.2	Diffusion: Lagrangian framework . . . . .	7
4.3	The mean flow . . . . .	8
4.4	Shear dispersion . . . . .	8
4.5	Lagrangian Chaos . . . . .	9
<b>5</b>	<b>Kinematic Model</b>	<b>11</b>
5.1	Methods . . . . .	11
5.2	Results and discussion . . . . .	12
5.2.1	Shear and tides . . . . .	12
5.2.2	Tides and eddies . . . . .	12
5.2.3	Shear, tides and eddies . . . . .	14
5.2.4	Influence of shear . . . . .	16
<b>6</b>	<b>Labrador Sea</b>	<b>19</b>
6.1	Methods . . . . .	19
6.1.1	The Labrador Sea . . . . .	19
6.1.2	Drifter description and data processing . . . . .	21
6.1.3	Visser method for calculating the diffusivities . . . . .	22
6.1.4	Davis method . . . . .	23
6.1.5	Simulated trajectories . . . . .	24
6.1.6	Scale analysis . . . . .	24
6.2	Results . . . . .	25
6.2.1	Timescale analysis . . . . .	25
6.2.2	Drifter observations . . . . .	27
6.2.3	Parcels simulation . . . . .	29
<b>7</b>	<b>Discussion</b>	<b>31</b>
7.1	Observations vs simulation . . . . .	31
7.2	Drifters and water particles . . . . .	31
7.3	Integral Time Scale . . . . .	32
7.4	Seasonality and interannual variability . . . . .	32
7.5	Effect of tides . . . . .	32
7.6	Application of kinematic model . . . . .	33
7.7	Outlook . . . . .	33
<b>8</b>	<b>Conclusion</b>	<b>35</b>
<b>9</b>	<b>Bibliography</b>	<b>36</b>

### 3 Introduction

Knowledge of the spreading of tracers in the ocean is of importance for many different research topics as well as for practical applications. Not only is there more and more plastic accumulating the global oceans, from which we do not know where it all ends up, also the knowledge of how nutrients or other tracers are spreading or where oil ends up can be beneficial for cleaning actions, the fishing industry and climate monitoring. The spreading of these tracers can be modelled by global ocean models, these models often have resolutions in the order of 1 degree, therefore solving the global circulation patterns, but not the submesoscale or even mesoscale eddies (Kirtman et al., 2012). For the spreading of tracer material, these eddies are important. Therefore, a common solution is to assume that the transport of a passive tracer is caused by two independent processes; advection, caused by the mean flow, and eddy diffusion or just diffusion. Advection is in this case the transport caused by the flow field that is fully resolved by the model. Depending on the grid size and temporal resolution of the model this is mainly the large scale circulation pattern. Diffusion is in this case a parameterization of all non-resolved subgrid-scale processes. Although the processes involved are strictly not diffusive in the traditional sense of the word, the expression is derived from molecular diffusion, where on certain time scales ocean material exhibits the same behaviour as Brownian motion (Taylor, 1922). Eddy diffusion thus causes an irreversible spreading that can be described by Fick's law and it assumes that material moves in a 'random' way from high to low concentration.

The main cause for this 'random' diffusion is turbulent motion caused by eddies, therefore it is often called eddy diffusion. The rate of diffusion is characterized by a coefficient that we call the eddy diffusivity, or just diffusivity. Besides the transport by eddies, also other processes may contribute to the diffusion term, like tides and inertial oscillations. Despite these two processes being periodic, they still can cause a spreading because they are often accompanied by rectified currents and they can interact with other velocity components. Furthermore, the diffusion may be enhanced or reduced greatly by the presence of shear in the mean flow. Because of the interaction of the diffusion with the advection and the tides, this can result in diffusivities that are far greater and more anisotropic than one would expect from eddy activity alone. In this study we also use the expression 'dispersion', where we mean the spreading of a material around their center of mass, not assuming anything about the processes causing this spreading.

In most previous studies (Davis, 1991; Zhurbas, 2003; Zhurbas et al., 2014; R hls et al., 2018) and in ocean models, the diffusivity is assumed to be isotropic and sometimes even constant over a large domain. This may be an appropriate assumption in the interior of the oceans where we expect shear gradients and tidal effects to be small, however in coastal regions and near boundary currents this does not seem to be a logical assumption. Diffusion is influenced by shear in the mean flow (Zimmerman, 1986), which gives rise to anisotropies. Furthermore, tides could play an important role in this diffusion as well, especially in combination with shear of the mean flow (Maas, 1989; Meyerj rgens et al., 2020). Therefore, especially in coastal regions, ocean models may not do well in reproducing the pathways of particles in the ocean. For knowing where a tracer might end up, for example plastic, oil or nutrients these coastal regions are however important and increasing our understanding of diffusion in these regions might also increase our ability of predicting the spreading of tracer material.

Traditionally the influence of the tides on the diffusion of a tracer was modelled with a stochastic model, where particles are subject to a deterministic signal, the tides, and a stochastic diffusion component. The combination of these may give rise to high effective diffusivities (Csanady, 1973). Zimmerman (1986) proposed however the concept of Lagrangian Chaos where particles are advected on a totally deterministic velocity field with different components; a tidal flow and a residual flow, consisting of eddies. Simulations showed that even though there is no stochastic component and there is only a relatively simple kinematic flow field, particle trajectories show chaotic behaviour, e.g. do not stay in an ordered formation but seem to move in a random way. In this way, high effective diffusivities can be reached, without the need of a stochastic component.

Eddy diffusivity can be studied in two different ways; from a tracer-based Eulerian framework (e.g. Bachman et al. (2020)) or from a particle-based Lagrangian framework (Taylor, 1922; Davis, 1991; Zhurbas et al., 2014; R hls et al., 2018). In this thesis we will use a Lagrangian framework to study eddy diffusivity. For Lagrangian studies we can use so-called drifters or floats, which are buoys that are drifting with currents on the ocean surface, sampling their locations. Alternatively, Lagrangian models can be used where virtual particles are advected on known velocity fields. In our study we will use both these methods, so the observational data can be compared with model data. A more elaborate description of the drifters and the methods we use will follow in the methods section. The study of eddy diffusivity via particle-based Lagrangian statistics can again be categorized in two different parts: single-particle statistics and multiple-particle statistics. Here multiple-particle statistics uses the relative distances between different particles. It has the advantage of not being influenced by a spatially uniform mean flow (LaCasce, 2008) and therefore would be the easiest option. Yet although constant flows do not influence these relative distances, shear in the mean flow still does. The

downside of this method is that it needs drifters to be released in pairs or clusters and this data is not so widely available. An alternative method for this would be to use so called 'chance pairs' where one makes use of drifters that are located close to each other by 'chance', thus acting as a pair of drifters, however, since drifters are covering the whole global ocean, this does not occur so regularly. Of course the abundance of chance pairs depends on the definition of a chance pair, but considering that at the moment there are about 1500 drifters floating in all of the world oceans, the chance that two drifters get together at a distance of a few kilometers is small.

Because of these drawbacks, single-particle statistics are more regularly being used (LaCasce, 2008). Research in this field has already been carried out extensively and the theory was already developed a century ago, by Taylor (1922), who described that the diffusivity can be calculated by integrating the autocorrelation of the velocity of a particle. This theory has been generalized and elaborated by Davis (1987). Davis (1991) does however assume the diffusivity to be isotropic.

In this study we will investigate the influence of the tides on the anisotropic nature of the diffusivity in the horizontal plane, obtained by Lagrangian analysis of surface drifters and of model simulations. We will focus on the following research question: What is the influence of the tides on the anisotropy of the diffusivity tensor.

To answer this question we start by using an idealistic kinematic model to investigate how the interaction between tides, eddies and shear cause the dispersion of particles and what this means for the diffusivity. We will then use the concepts and results that we obtained from this study to interpret observational and numerical results of more realistic situations. We will do this by limiting our study area to the Labrador Sea, a region that we chose due to the combination of a large tidal range and a high coverage of data. Here we will use data from surface drifters to calculate diffusivities in two different ways, one introduced by Visser (2008), which assumes the diffusivity being isotropic. The other method was introduced by Davis (1991) and even though Davis (1991) does assume isotropy and therefore only looks at one component of the diffusivity tensor, we will look at the entire diffusivity tensor, thus taking anisotropic effects into account. We will compare the results of these observations to results obtained by Lagrangian particle modelling. For this modelling we use the Parcels v2.2 Lagrangian framework (Delandmeter and van Sebille, 2019) and surface current data from the Surface and Merged Ocean Currents (SMOC) from the Copernicus Marine Environmental Monitoring Service (CMEMS). In this dataset the ocean currents are divided into different components for the general circulation, tidal currents and Stokes drift. This enables us to compare model runs with and without tides with the observations, thereby showing the influence of the tides on the diffusivity tensor. Previous studies suggested that barotropic tides do not have a large influence on the accumulation zones and transport patterns of microplastics in the open ocean, but also that it could affect local transport in coastal regions (Sterl et al., 2020). Therefore we expect that, especially on the continental shelf and the shelf edges, the tides will also have an effect on the diffusivity tensor, making it more anisotropic.

The code used for this thesis can be found at: [https://github.com/TBovenschen/Master\\_thesis.git](https://github.com/TBovenschen/Master_thesis.git)

## 4 Theory

### 4.1 Diffusion: Eulerian framework

To model the evolution of the transport of a tracer, models often make use of the tracer equation (1). This equation results from mass conservation, assuming incompressibility and using Reynolds decomposition

$$\frac{\partial C}{\partial t} + \mathbf{U} \cdot \nabla C = -\nabla \cdot \langle \mathbf{u}'c' \rangle \equiv \nabla \cdot (\boldsymbol{\kappa} \nabla C). \quad (1)$$

Here  $C$  is the concentration of a passive tracer,  $\mathbf{U}$  is the time-averaged velocity and  $\boldsymbol{\kappa}$  is the diffusivity, which can be a scalar for isotropic diffusion, or a tensor in case of anisotropic diffusion. The primes indicate deviations from the mean values and  $\langle \rangle$  indicates the ensemble average. In this equation we divide the transport processes into two different terms: advection and diffusion. Here advection is caused by the mean flow, this does not contribute to any mixing; a patch of tracer material would not be 'deformed' by this, it would only be transported as a whole. The diffusion term parameterizes all non-resolved subgrid-scale processes that cause mixing by using the closure hypothesis that  $-\langle \mathbf{u}'c' \rangle = (\boldsymbol{\kappa} \nabla C)$ . By dividing the transport of the tracer into these two terms, we implicitly assume that these processes can be separated in time scales, the long time scale of the order of months or years causes the mean flow and diffusion takes place on a time scale of hours to days. In reality this assumption does not seem to be valid, since timescales in the ocean will consist of an entire continuous spectrum, where there is not a clear distinction between short and long time scales (Zang and Wunsch, 2001), but for practical reasons we still make it.

### 4.2 Diffusion: Lagrangian framework

The diffusivity as present in the tracer equation (1), can be calculated from Lagrangian data, as first described by Taylor (1922). Say we have a patch of particles that are released from a certain location. The second moment, or variance, of the particle displacements of this patch is what we call the 'absolute dispersion' (LaCasce, 2008):

$$\langle X^2 \rangle = \langle (\Delta x - \Delta x_{mean})^2 \rangle. \quad (2)$$

Here  $\langle \rangle$  is the ensemble average over all particles. Absolute dispersion is a measure of how much particles have spread around their starting position. The time derivative of this absolute dispersion, divided by two is defined as the absolute diffusivity:

$$\kappa(t) \equiv \frac{1}{2} \frac{d}{dt} \langle X^2 \rangle. \quad (3)$$

Taylor (1922) showed that for stationary and homogeneous flows this can be rewritten into a function of the velocity and the autocorrelation of this velocity:

$$\kappa(t) = v_{rms}^2 \int_0^t R(\tau) d\tau, \quad (4)$$

where  $R(\tau)$  is the autocorrelation of the velocity and  $v_{rms}$  the root mean square velocity of the particle:

$$R(\tau) = \frac{\langle v(\tau)v_0 \rangle}{\sqrt{\langle v(\tau)^2 \rangle \langle v_0^2 \rangle}}, \quad (5)$$

where  $v_0$  is the velocity at  $\tau = 0$  Equation (4) only holds for stationary conditions, but was generalized by Davis (1991) for inhomogeneous and instationary flows:

$$\kappa(t) \equiv \frac{1}{2} \frac{d}{dt} \langle X^2 \rangle = \langle X(t)u(t) \rangle = \int_0^t \langle u(X, t)u(X, \tau) \rangle d\tau, \quad (6)$$

here the diffusivity is dependent on the duration  $t$  of the displacement. However, from equation (4) we can already see that the diffusivity might reach a constant asymptotic limit, as long as the autocorrelation of the velocity goes to zero after a certain time.

Now, to connect this Lagrangian diffusivity to the diffusivity that we have in the tracer equation (1), imagine we have a patch of particles being released at a certain location. Let us now assume that the particle movement can be described with a first order Markov process (a random walk) as described by the following equation:

$$dx = udt + \sqrt{2\kappa}d\eta. \quad (7)$$

The displacement of the particles is thus caused by a 'deterministic drift' term and a stochastic term. Here  $d\eta$  is a Wiener increment, it is a random increment which has a Gaussian distribution and variance  $dt$ :  $\langle d\eta \rangle = 0$



and  $\langle d\eta^2 \rangle = dt$ .  $\sqrt{2\kappa}$  indicates the amplitude of the stochastic process and  $\kappa$  is the same as the absolute diffusivity in equation (3) as we will show below.

The time evolution of the probability density function  $p(x, t)$  for where particles end up can then be described by a stochastic differential equation, the so-called Fokker-Planck equation (Visser, 2008):

$$\frac{\partial p}{\partial t} = -\frac{\partial}{\partial x}(up) + \frac{\partial^2}{\partial x^2}(\kappa p), \quad (8)$$

where  $p$  is the probability that a particle is found on a certain location at a certain time. This Fokker-Planck equation can be related to the tracer equation (1), since for a large number of particles the probability that particles end up at a certain location is actually equivalent to the concentration.

If, for clarity, we take the discretized form of equation 7:

$$x(t + \Delta t) - x(t) = u\Delta t + \sqrt{2\kappa}\Delta\eta. \quad (9)$$

And now if we take the second moment (variance) of the displacement of the particles (as given by equation 9) and take the time derivative of it, keeping in mind the characteristics of the Wiener increment, we get:

$$\lim_{\Delta t \rightarrow 0} \frac{\langle (x(t + \Delta t) - x(t))^2 \rangle}{\Delta t} = \lim_{\Delta t \rightarrow 0} \frac{\langle (u\Delta t + \sqrt{2\kappa}\Delta\eta)^2 \rangle}{\Delta t} = \lim_{\Delta t \rightarrow 0} \left( \frac{\langle u^2 \Delta t \rangle}{\Delta t} + \frac{\langle 2\kappa \Delta\eta^2 \rangle}{\Delta t} + \langle 2u\sqrt{2\kappa}\Delta\eta \rangle \right) = 2\kappa. \quad (10)$$

Thus, as long as the trajectories of particles can be described as a random walk and we assume the tracer equation is similar to a Fokker-Planck equation, the time derivative of the variance of the displacement of the particles divided by two is the diffusivity as we find it back in the tracer equation.

The diffusivity, as present in the tracer equation, can therefore be calculated purely by using the displacement and/or the velocity data from trajectories. The mean flow affects this value for the absolute diffusivity. Therefore, the mean flow and the displacement by the mean flow have to be subtracted from the total velocities and displacements first (Davis, 1982). If we use the different velocity and displacement components in the zonal and meridional direction separately, this method results in a diffusivity tensor. This tensor can be separated in a symmetric and an asymmetric part. The asymmetric part does not contribute to the irreversible mixing associated with diffusion (Griffies, 1998) and therefore for calculating the diffusivity only the symmetric part is considered. For calculating the displacement, a typical time scale is needed however. This timescale should be larger than the integral time scale (ITS) or decorrelation time scale, e.g. the time which it takes for the velocity to be totally decorrelated. We use this time scale because we assume the trajectories to be a random walk. In a random walk the velocity in each consecutive segment of the trajectory is 'random', thus not correlated with the velocity in the previous segment. Therefore, to make this approximation we have to take large enough intervals, so the velocity is indeed decorrelated.

### 4.3 The mean flow

The mean flow is often calculated directly from drifter statistics (Davis, 1991; Jakobsen, 2003; Zhurbas et al., 2014). By binning observations and averaging over certain grid cells, mean velocities are obtained. Since the period over which observations are used and averaged can be of the order of months to years, the flow is assumed to be stationary. Although useful, because only Lagrangian statistics are necessary, this method does have some disadvantages: One needs a lot of observations to get proper temporal means that are not influenced by eddies or other short term effects. Therefore often the time scale of the averaging is taken to be on the order of years, thus not accounting for seasonality or inter-annual variability. Furthermore, the mean depends on the amount of observations and therefore certain regions may be undersampled, due to a non-uniform distribution of the drifters. To prevent this bias one could however also use the Eulerian means from ocean models or other observations like satellite data, stationary current meters and floats.

### 4.4 Shear dispersion

The dispersion of particles can be greatly increased by the presence of shear in the mean flow (Taylor, 1953; Okubo, 1968). Imagine a simple shear flow in the zonal direction with a small, stochastic diffusive process in the meridional direction. Particles will move in the zonal direction with different speeds, so the interaction with diffusion in the meridional direction will give rise to an enhanced dispersion into the direction of the flow. This process is illustrated in figure 1. The resulting enhanced dispersion results in a 'diffusivity' that is anisotropic.

When calculating the diffusivity tensor from Lagrangian data, the result is influenced by this shear effect, because one calculates the effective diffusivity. Previous studies often correct for this 'shear bias', for example by looking only at the minor principle component of the diffusivity tensor (e.g. Zhurbas (2003), Zhurbas

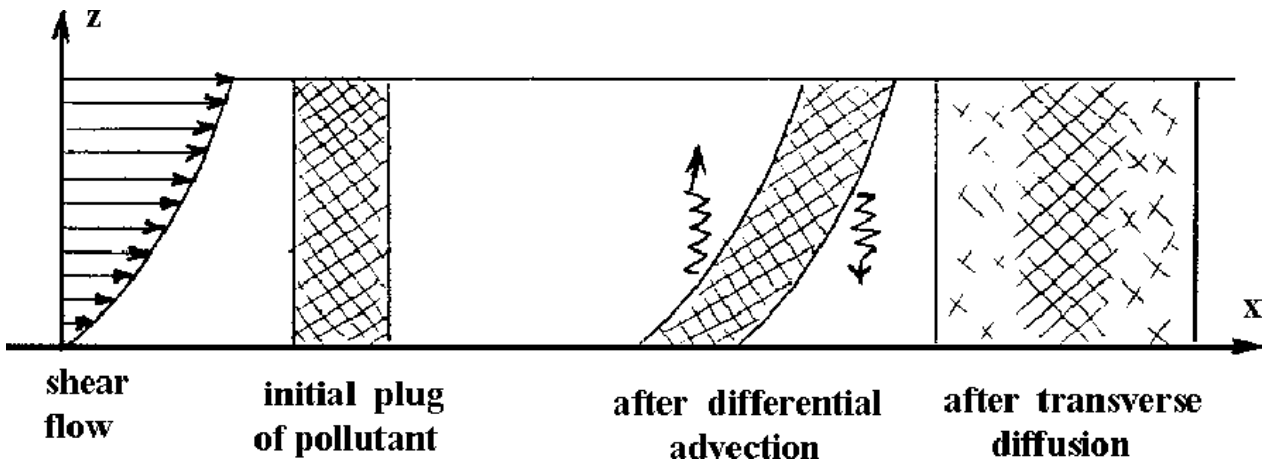


Figure 1: An illustration of how the combination of a sheared flow with a stochastic component in the cross-direction results in an along-flow dispersion (Cushman-Roisin, n.d.)

et al. (2014), and Rühls et al. (2018)). The idea of this is that the shear only enhances the diffusion in the along-flow direction, therefore only the major principle component of the diffusion tensor is affected by the shear effect. The minor principle component is thus taken as the ‘real’ diffusion, which is assumed to be isotropic. The question then arises however whether we are interested in the ‘real diffusivity’, only caused by eddies and minor scale turbulence, or in the ‘effective diffusivity’, including the effects of shear. This depends on the applications where we want to use the diffusivity for. If for example, we want to use the diffusivity to improve the modelling of the spreading of particles in ocean models, it mainly depends on the resolution of the model. The diffusion term incorporates all non-resolved processes that cause spreading of particles, ranging from small scale turbulence to mesoscale eddies. Shear within a gridcell will not be resolved by an ocean model, and therefore the shear dispersion has to be incorporated in the diffusion term. The amount of shear that is present does however depend on the size of the gridcells and thus on the resolution of the model.

## 4.5 Lagrangian Chaos

The effective diffusivity is not only influenced by shear, but also by tides. Even though tides are a deterministic signal, they are often not resolved in ocean models and therefore it is reasonable to include the effects in the diffusion term. Tides themselves do not have a dispersive effect on particles, since it is an oscillating current. Still, they might enhance the diffusion. This is due to the interaction of the oscillating current with other features that are present in the residual currents, for example eddies or small scale turbulence (Zimmerman, 1986). Traditionally this effect was described as being a ‘cascade’ of shear dispersion effects, where tidal effects create a shear component in the flow. In combination with a small stochastic diffusion process (turbulence) in the vertical or lateral direction, this can create high effective diffusivities in the lateral direction, in the same way as described in the previous section (Csanady, 1973; Zimmerman, 1986).

However, a different way of describing the process is by the concept of ‘Lagrangian chaos’. This means that even though the Eulerian flow field is completely deterministic, due to the interaction of different components of the flow with different time and length scales, the trajectories might exhibit chaotic trajectories. This chaos can already occur with simple kinematic flows, that consist of only sines and cosines (Regier and Stommel, 1979; Zimmerman, 1986). If particles are moving in a chaotic way, this means that they are causing dispersion and we could describe the trajectories as a random walk. Therefore we can also describe the spreading as a diffusive process and calculate the diffusivity. To model this effect, previous studies have looked at simple kinematic models, where a tidal current is superposed on a residual flow field. The idea of this is that due to complex geometries in areas where there is a tidal current, a residual flow field is created with features of different length and time scales. Regier and Stommel (1979) and Beerens et al. (1994) modeled the interaction of these currents with the tides for simple analytical flow fields and the idea has also been applied to more realistic models of for example the Dutch Wadden Sea (Ridderinkhof and Zimmerman, 1992). For the simple analytical flows, the residual currents are usually modelled as a field of stationary eddies that are rotating clockwise and anti-clockwise alternately. From these studies we can conclude that the amount of chaotic behaviour, and thus the amount of spreading of the particles, depends mainly on the ratio  $\nu$  of the amplitude of the tidal velocity and the eddy velocity and on the ratio  $\lambda$  of the tidal excursion and the eddy diameter. Zimmerman (1986) and Beerens et al. (1994) showed that the rate of spreading in the direction of the tidal

excursion is greatest when the tidal velocity and the eddy velocity are approximately equal. Furthermore they showed that there is an oscillatory dependence of the rate of spreading on the ratio of the tidal excursion length and the eddy diameter.

In this study we will continue on this research by adding a new parameter: the angle  $\theta$  that the tides make with the eddy field. Furthermore, we add an extra component to the flow; a linear shear flow. The addition of the shear field is specially applicable to the Labrador Sea, since here we often have strong shear gradients near the boundary currents. By investigating the interaction of the tides, with eddies and a shear flow and by changing the angle of the tides we can obtain more knowledge of how this interaction influences diffusion in the ocean.

## 5 Kinematic Model

### 5.1 Methods

To better understand the interaction between the tides and shear or eddies, we created a kinematic model where we simulate the transport of virtual particles on different kind of flows. For the flow field we use equations (11), where  $u$  is the velocity in the  $x$ -direction and  $v$  the velocity in the  $y$ -direction

$$u(x, y, t) = A_e \cos(x) \sin(y) + A_t \cos(\theta) \sin(t) \quad (11a)$$

$$v(x, y, t) = -A_e \sin(x) \cos(y) + A_t \sin(\theta) \sin(t) + sx. \quad (11b)$$

All parameters and velocities in these equations are made dimensionless. These equations consist of three terms, describing different processes. The first term represents a stationary eddy field, where  $A_e$  is the amplitude of the eddy velocity. The eddies form a checkerboard with clockwise and anti-clockwise rotating cells (figure 2a). The second term in both equations is an oscillating flow, only depending on time, representing a tidal flow with only one component (figure 2b).  $A_t$  is the amplitude of the tidal velocity and  $\theta$  is the angle that the tidal flow makes with the  $x$ -axis. The last term, only present in the equation for  $v$  represents a shear flow, that increases linearly with increasing  $x$  (figure 2c). Here  $s$  is the 'slope' of the shear flow; e.g. a measure of how fast the flow is increasing with increasing  $x$ .

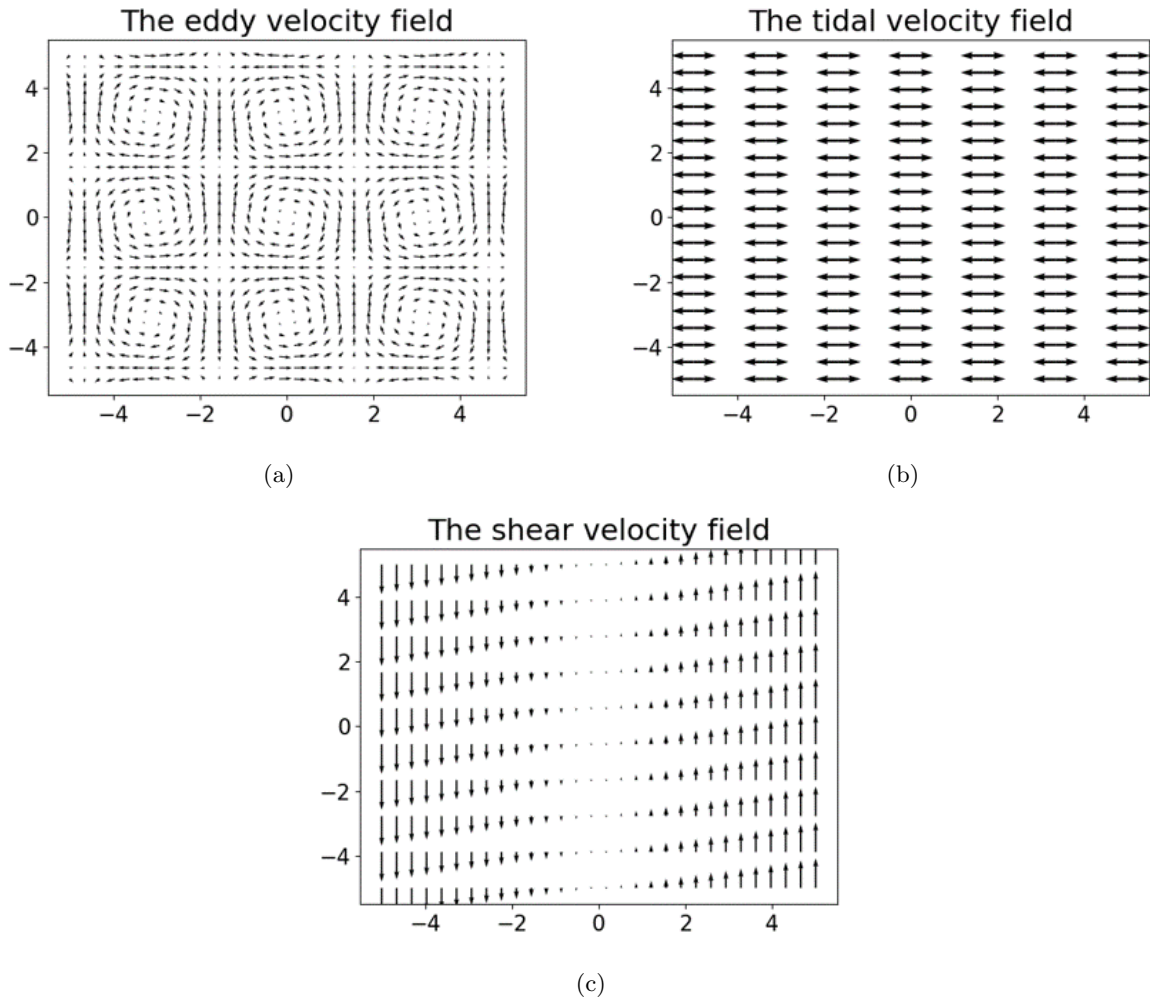


Figure 2: The three velocity components of the kinematic model. a) is the eddy velocity field, b) the tidal velocity field and c) the shear field.

In this velocity field we released a patch of 30 by 30 particles in a square, with release locations between  $x = [-1, 1]$  and  $y = [-1, 1]$ . These particles we integrated over time with a fourth-order Runge-Kutta scheme. As a measure of the spreading we used the variance in the displacement (the absolute dispersion), for both  $x$  and  $y$  separately. In order to investigate which configurations caused Lagrangian chaos and which did not, we first ran the model with the different components switched on and off. For every simulation we observed

whether the particles stayed in an ordered formation or moved in a seemingly random way, indicating chaos. To investigate the influence of the angle that the tides make with the  $x$ -axis, we also ran the model with only the eddies and tides, with different values for  $A_t$  and  $\theta$ . The diffusivity can be calculated by taking the time derivative of the absolute dispersion (section 4.2). Therefore, by observing the development of the absolute dispersion over time, we can also see in what kind of diffusive regime we are. A constant dispersion means that the diffusivity is zero. A linearly increasing dispersion means the diffusivity stays constant and a quadratic increasing dispersion means the diffusivity increases linearly.

Subsequently, we ran the model several times with all terms switched on, but with different values for the parameters  $s$ , to see what the influence is of the shear is on the rate of dispersion. In the  $y$ -direction the dispersion is dominated by shear-dispersion but we only want to look at the influence of the interaction between tides, eddies and shear. Therefore we also did a simulation where we advected the particles on a shear flow only, as well as on the total velocity field. By subtracting the dispersion in the  $y$ -direction of the pure shear flow from the total velocity field, we could see the influence of the other terms in combination with the shear flow.

## 5.2 Results and discussion

### 5.2.1 Shear and tides

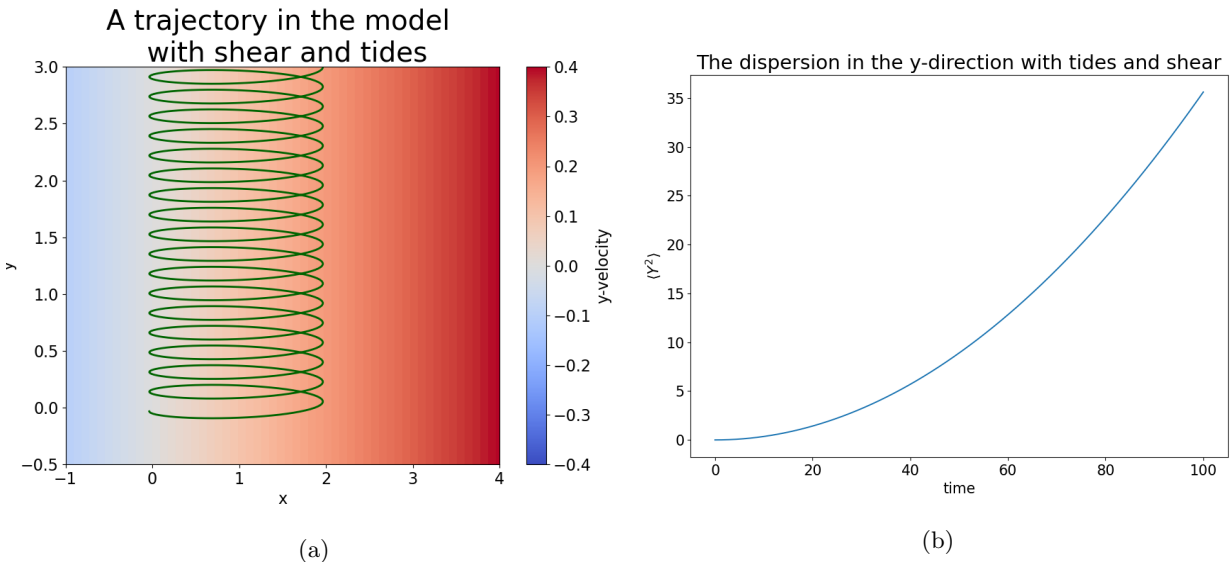


Figure 3: The results for a simulation with only the tides and the shear components turned on. Figure a) shows a trajectory of one of the particles in the model. b) shows the dispersion in the  $y$ -direction over time. The parameters for the model were:  $A_t = 1$ ,  $s = 0.1$ ,  $\theta = 0$

The model simulation with the tidal and shear components shows a quadratic increase in the dispersion in the  $y$ -direction (figure 3b). The particles oscillate due to the tides and the patch is stretched by the shear effect, in figure 3a we can see one trajectory of a particle. This effect is similar to what we know as shear dispersion as introduced by Young et al. (1982). The particles stay in an ordered formation, just being stretched by the shear, but no chaos is present. Superposing a tidal flow that is normal to this flow does not alter this effect, since the tidal flow is purely in the  $x$ -direction, the dispersion in the  $x$ -direction oscillates, but does not alter the dispersion in the  $y$ -direction.

### 5.2.2 Tides and eddies

For the configuration with a tidal flow in the  $x$ -direction superposed on an eddy field, the particles are spreading in a chaotic fashion in the  $x$ -direction. In figure 4 the trajectory of one particle is shown. We can see the particle is oscillating in the  $y$ -direction and over time it moves in the  $x$ -direction. The trajectory already looks rather chaotic. In the  $x$ -direction the dispersion increases exponentially as can be seen in figure 5a. This result is in line with the result of Zimmerman (1986), who states that the interaction of tides with a residual current (eddies) can create a deterministic chaos, resulting in an effective diffusion, that depends on two ratios; the ratio of the tidal velocity to the eddy velocity and the ratio of the tidal excursion to the eddy diameter. Since there is no flow in the  $y$ -direction, other than the eddies, the particles stay trapped in their

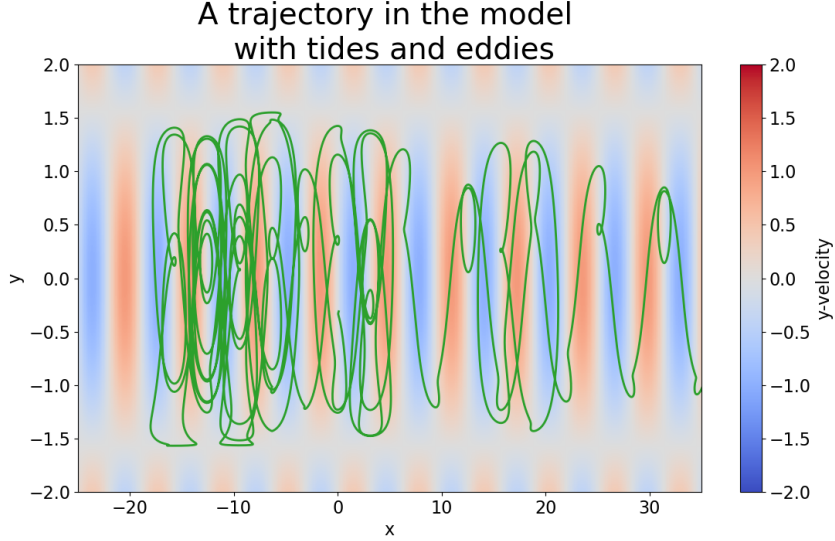


Figure 4: The trajectory of a single particle in the kinematic model with the eddy and tidal components.  $A_t = 1$ ,  $A_e = 1$ ,  $\theta = 0$ . The colors indicate the x-velocity of the eddy field on which the particles are advected.

starting eddy in the  $y$ -direction and the dispersion in the  $y$ -direction therefore oscillates around a constant value (figure 5b).

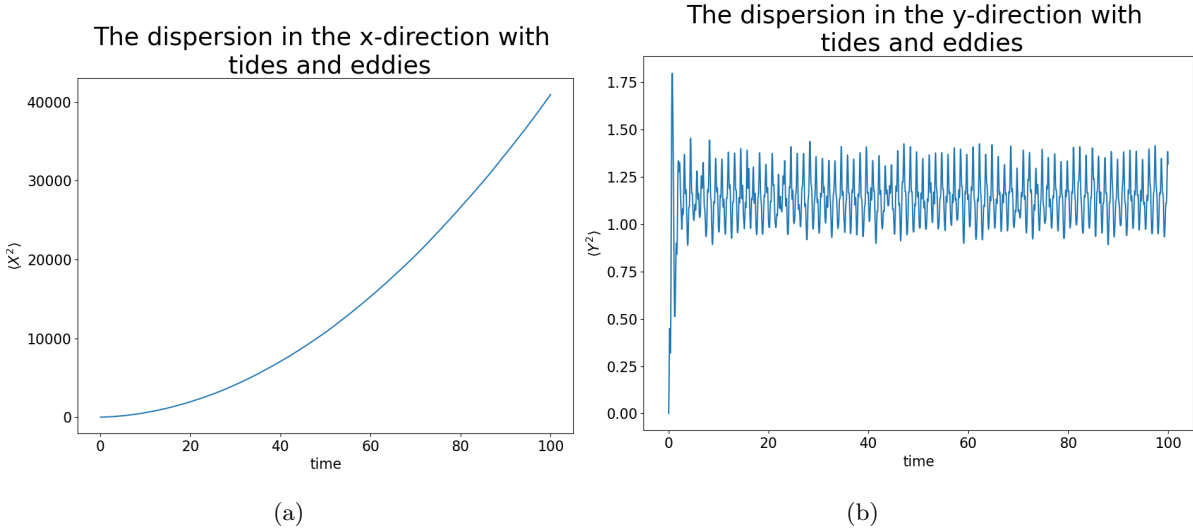


Figure 5: The dispersion in the  $x$ -direction (a) and  $y$ -direction (b) for a simulation with tides and eddies.  $A_t = 1$ ,  $A_e = 1$ ,  $\theta = 0$ ,  $s = 0$

For testing the dependence of the spreading on the parameters  $A_t$  and  $\theta$ , we looked only at the  $x$ -dispersion. Running the model many times with different parameters gave many different quadratic growing curves. Quadratic growth of the dispersion would mean that the diffusivity grows linearly, resulting in an anomalous diffusion, comparable with what results from shear dispersion. Why the dispersion grows quadratically as a result of the tides and eddies we do not exactly know. This could be investigated in further studies. Assuming the dispersion grows quadratically, we fitted the resulting curves with the following function:

$$f(t) = bt^2. \quad (12)$$

Where we determined the parameter  $b$ , which we call the growth factor. This growth factor is plotted in figure 6. As we can see the parameters are not independent, thus giving different configurations with high spreading rates in the  $x$ -direction, depending both on  $\theta$  and  $A_t$ . We can see that for  $\theta = 0$ , the growth rate of the dispersion is maximum when  $A_t$  is approximately 1, this coincides well with studies from Zimmerman (1986) and Beerens et al. (1994), stating that the dispersion is maximum when the eddy velocity is approximately equal to the tidal velocity ( $A_e = 1$  in this case, thus  $A_t$  gives the ratio of the tidal velocity with eddy velocity).

However, when we change the angle of tides with the  $x$ -axis, this picture changes. With  $\theta = 45$  degrees, there are several maxima for different values of  $A_t$ , namely for  $A_t = 1$ ,  $A_t = \sqrt{2}$ ,  $A_t = 2$  and  $A_t = \pi$ . The fact that the dispersion is maximum for different values of  $A_t$  can be explained conceptually with the idea of a 'cake walk', where there are different oscillating escalators next each other. By stepping from one escalator to another at the right pace, one can move in a certain direction. Now one can also imagine that this process is most efficient when the excursions of the oscillations are on the same order of magnitude and when the velocities with which the different escalators move are of similar magnitude. This concept might also explain why the maxima of the dispersion are present at different values for  $A_t$  when the angle of the tides with  $x$ -axis changes. The fact that there are several maxima for the spreading rate when the angle is 45 degrees might be explained by the idea that when a particle moves along the  $x$ -axis through the eddies, it stays trapped in one line of eddies, if we see the eddy field as a checkerboard, it only moves in one line of the fields, like a rook moves in chess. The only length scales that the particles encounter are the diameter of the eddies ( $\pi$ ) and the tidal excursions ( $A_t$ ). When the angle is 45 degrees, the particles are however not stuck to one line of eddies, but because there is now a tidal component in both the  $x$ - and the  $y$ -direction, they can move in different lines of eddies. Therefore one can imagine that the maxima also occur on different values of  $A_t$ . In fact, the values of  $A_t$  that give maxima in the growth factor might be explained by the scales of the different flow fields;  $A_t = 1$  gives a tidal amplitude that is exactly the same as the eddy amplitude, as showed by Zimmerman (1986), this gives a maximum in the spreading rate.  $A_t = \pi$ , gives the highest spreading rates. This values corresponds to a tidal excursion that is exactly the same as the eddy diameter, therefore it is not surprising that also this gives a high spreading rate. For  $A_t = 2$ , goes the same idea as for  $A_t = 1$ , but the tidal amplitude is now exactly twice the eddy velocity amplitude. The maximum at  $A_t = \sqrt{2}$  can be explained because this results in a tidal amplitude of 1 in the  $x$ -direction (following from Pythagoras, since  $\theta = 45$  degrees). Thus the tidal amplitude in the  $x$ -direction is the same as the eddy amplitude.

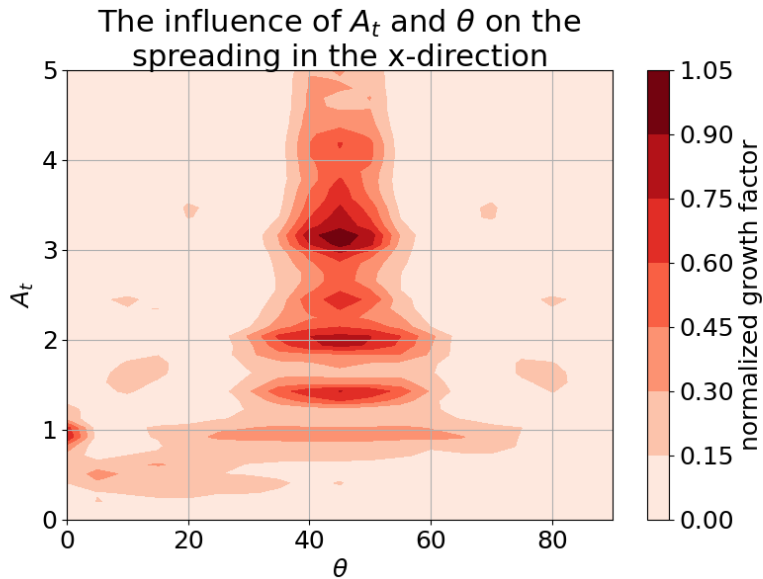


Figure 6: The dependence of the rate of spreading in the  $x$ -direction on the amplitude of the tides ( $A_t$ ) and the angle of the tides with  $x$ -axis ( $\theta$ ). The colors indicate the quadratic growth factor of the dispersion in the  $x$ -direction.  $A_e$  has a fixed value of 1.

### 5.2.3 Shear, tides and eddies

To continue on previously done research, we added a background shear-flow to the previously described flow field (the last term in (11b)). The simulation therefore now consists of three components: a tidal component, an eddy component and a shear component. In this simulation the particles show chaotic behaviour, but unlike when there is no shear flow, after a while the particles seem to stop spreading in the  $x$ -direction, this can be seen also in figure 7a, the dispersion in the  $x$ -direction shows a kink, after which it increases at a lower rate then before.

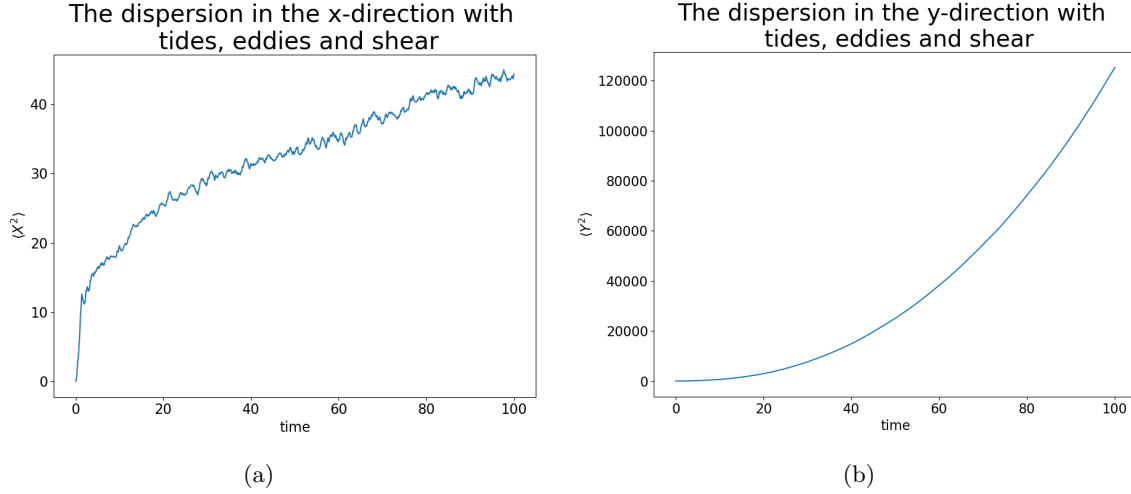


Figure 7: The dispersion of the displacement in the  $x$ -direction (a) and  $y$ -direction (b) for a simulation with tides, eddies and shear.  $A_t = 1$ ,  $A_e = 1$ ,  $\theta = 0$ ,  $s = 0.1$ .

In figure 8 we can see two trajectories of particles that were advected. Here also see that for low  $|x|$ , the particles move in a chaotic way, but for higher  $|x|$  the particles stop moving further in the  $x$ -direction, only showing an oscillation.

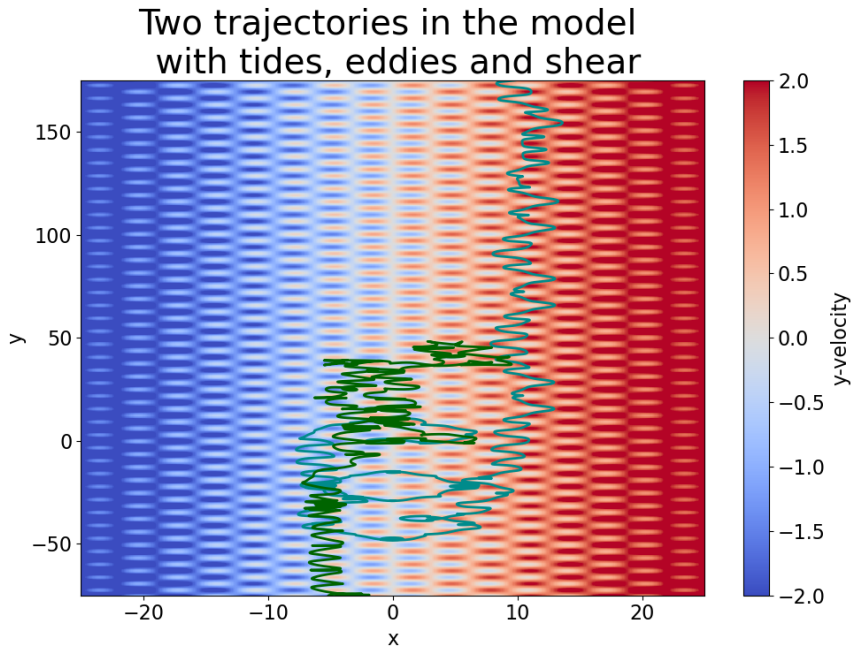


Figure 8: Two trajectories of particles released in the kinematic model. The particles were released at  $[-0.3, 0.3]$  (green),  $[-0.2, -0.3]$  (orange) and  $[-0.1, -0.3]$  (blue). The parameters for the model are:  $A_t = 1$ ,  $A_e = 1$ ,  $\theta = 0$ ,  $s = 0.1$ .

The spreading in the  $y$ -direction is dominated by shear dispersion; because of the differences in the  $y$ -velocities in the background shear flow, the particles are quickly spreading into this direction. Since we are mainly interested in the effect of the tides, in combination with the eddies and shear flow, we have subtracted the spreading that is caused by the shear flow only. We have done this by running a simulation with only shear flow and calculating the resulting dispersion in the  $y$ -direction. By subtracting this dispersion from the dispersion that resulted from a run including eddies and tides, we can see the difference in the spreading in the  $y$ -direction that is directly caused by the interaction between the different velocity components (figure 9).

Even when the dispersion resulting from the shear is subtracted from the dispersion from the total flow, the resulting dispersion in the  $y$ -direction increases exponentially. In fact, the spreading is only slightly less than when the shear flow is not subtracted. This result can be explained by comparing to the dispersion in



the  $x$ -direction; the tides in combination with the eddies cause a spreading in the  $x$ -direction. This increases the distance along the  $x$ -direction between the different particles and therefore also increases the difference in  $y$ -velocity. This bigger difference in  $y$ -velocity thus causes the shear dispersion to be much larger.

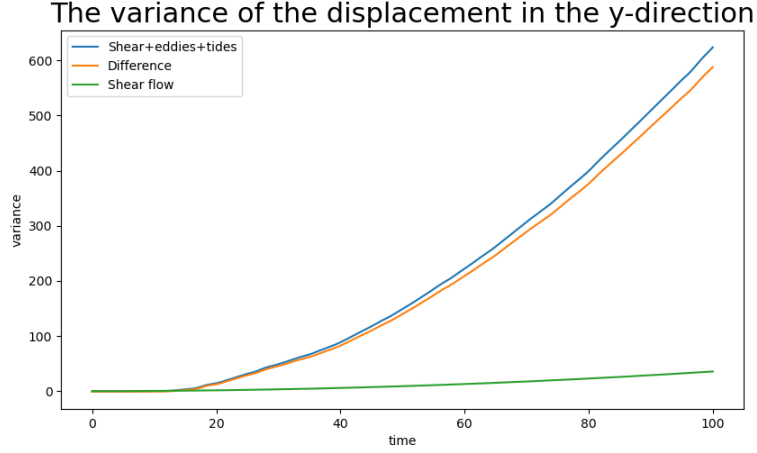


Figure 9: The dispersion in the  $y$ -direction for a simulation with shear, eddies and tides (blue). The green line is a simulation with only shear flow and the orange is the difference between the two simulations. The equation parameters are:  $A_e = 1$ ,  $A_t = 1$ ,  $\theta = 0$ ,  $s = 0.1$ .

#### 5.2.4 Influence of shear

Figure 10 shows the dispersion in the  $x$ -direction for a simulation where the ‘slope’ of the shear is varied. As can be seen from the figure, the dispersion increases less when the slope of the shear is higher. Thus, if there is a higher shear in the background flow in the  $y$ -direction, there is less spreading in the  $x$ -direction. For large flow velocities in the  $y$ -direction, the particles are trapped in a line, only having small deviations in  $x$ . We can also see this in the trajectories in figure 8, where particles seem to move in a chaotic way, but as soon as  $|x|$  becomes too large, the particles are not spreading in the  $x$ -direction anymore, but only oscillate.

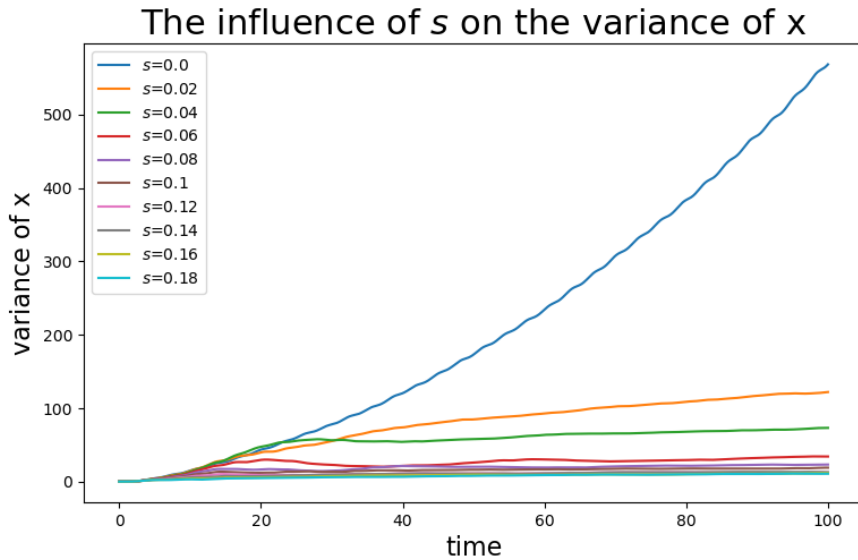


Figure 10: The dispersion of  $x$  for a simulation with eddies, tides and shear.  $s$  is varied in the different simulations.  $A_e = 1$ ,  $A_t = 1$ ,  $\theta = 0$ .

We think that this effect has not so much to do with the shear in the flow itself, but more with the magnitude of the background velocity. As soon as the background velocity is too high, the particles are being pushed through the eddy field very quickly, leaving no time for the eddies and the tides, to properly mix the particles.

If we look at the original equations, we can try to make some approximations to see what happens for large  $x$ :

$$u(x, y, t) = A_e \cos(x) \sin(y) + A_t \cos(\theta) \sin(t), \quad (13a)$$

$$v(x, y, t) = -A_e \sin(x) \cos(y) + A_t \sin(\theta) \sin(t) + sx. \quad (13b)$$

Now, for  $x \gg 0$ : (13b) can then be approximated by:

$$v(x, y, t) = sx. \quad (14)$$

Because the shear term is much greater than the eddy and tide terms. We can see now that  $v$  only depends on  $x$ , and thus,  $y$  grows linearly in time

$$y(x, t) = sxt, \quad (15)$$

this results indeed in quadratic growth of the dispersion in the  $y$ -direction Filling in this equation into equation (13a) gives:

$$u(x, t) = A_e \cos(x) \sin(sxt) + A_t \cos(\theta) \sin(t). \quad (16)$$

We see now that  $u$  is only dependent on  $x$  and  $t$ , we still can not solve this equation analytically, but numerically it is possible. We integrated the equation with an fourth order Runge-Kutte scheme, a timestep of 0.1 and for different initial values. In figure 11 we can see solutions of equation (16) for  $x(0)$  ranging from -20 to 20, parameters that we used in the model are the same as in figure 8;  $A_t = 1$ ,  $A_e = 1$ ,  $\theta = 0$ ,  $s = 0.1$ .

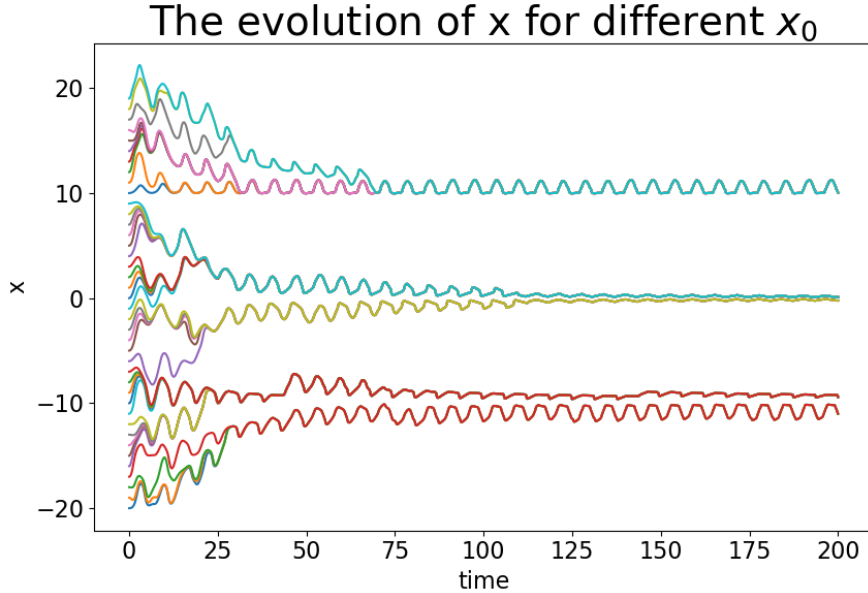


Figure 11: The evolution of  $x$  as a result of integrating equation (16) numerically. The different colors indicate different starting values ( $x_0$ ) for  $x$ .

As we can see,  $x$  oscillates through time, as we can expect from the equation. For all values of  $x_0$ ,  $x$  converges to a certain limit around which it oscillates. Interestingly, there seem to be different limits whereto  $x$  converges, depending on the starting value. The values of the different limits are -10, 0 and 10 for these values of  $x(0)$ . If we compare this to figure 8, we see that there indeed seems to be a limit for the particle at  $x = 10$ , where the particle only oscillates but does not move in the  $x$ -direction anymore. From the simplified equations (16) and (15), we can thus indeed deduce that after a certain time, particles stay in a certain line of eddies, not being able to move in the  $x$ -direction anymore, apart from an oscillation within the eddies. Note that the approximations we made are only valid for  $x \gg 0$ , thus the convergence limit at  $x = 0$ , is not realistic, because these approximations are not valid in this area.

The phenomenon where a background flow suppresses the mixing in the cross-flow direction, has already been observed before, for example in the Antarctic Circumpolar Current, where mixing in the interior of the current is smaller then expected (Ferrari and Nikurashin, 2010). According to mixing length theory, one would expect highest mixing and thus highest eddy diffusivities at the core of the current. However observations show that in the regions where the mean flow is highest, mixing is suppressed due to the propagation of eddies relative to the mean current (Klocker et al., 2012; Klocker and Abernathey, 2014). The mean flow

reduces the effective mixing length of the eddies, therefore also reducing the mixing itself. We think this is essentially also what is happening in our model. The background flow in the  $y$ -direction causes the particles to 'fly' over the eddy field, causing them only to oscillate in the  $x$ -direction but not spending enough time in the eddies to be properly dispersed by them.

The main ideas that we obtained from the study with our kinematic model are that tides in combination with eddies can cause a large enhanced and anisotropic diffusivity in the direction of the tidal excursion, depending on the length and velocity scales and the orientation of the tides and eddies. Furthermore, the inclusion of a shear flow can reduce the mixing in the cross-flow direction, but the interaction between tides, eddies and shear do cause an increased shear dispersion in the direction of the shear flow. We can use these ideas for our analysis of the diffusivities in the Labrador Sea, which follows in the next section.

## 6 Labrador Sea

### 6.1 Methods

#### 6.1.1 The Labrador Sea

The Labrador Sea is the sea enclosed by Canada on the West, Greenland at the Northeast and the Atlantic ocean at the Southeast. The East Greenland Current enters the sea from the east and continues as the West Greenland Current along the coast of Greenland. Within the Labrador Sea it follows a counterclockwise direction, leading back to the Atlantic Ocean. The time-averaged velocities are shown in figure 12.

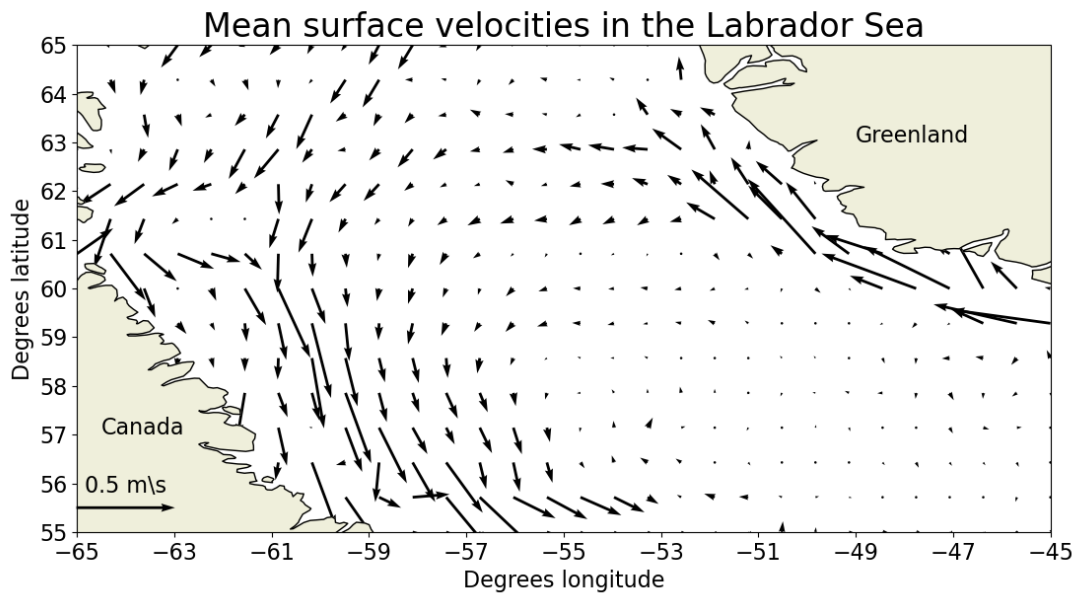


Figure 12: Temporal mean surface velocities in the Labrador Sea. The velocity data comes from the global reanalysis data of CMEMS and is the time-averaged velocity of monthly means from the period of 2012-2018. A large current enters the domain from the east (The West Greenland Current), then follows the coast of Greenland. A branch of this currents splits off at about 62 degrees latitude, making a counter-clockwise rotation to form the Labrador Current, leaving the domain again in the south.

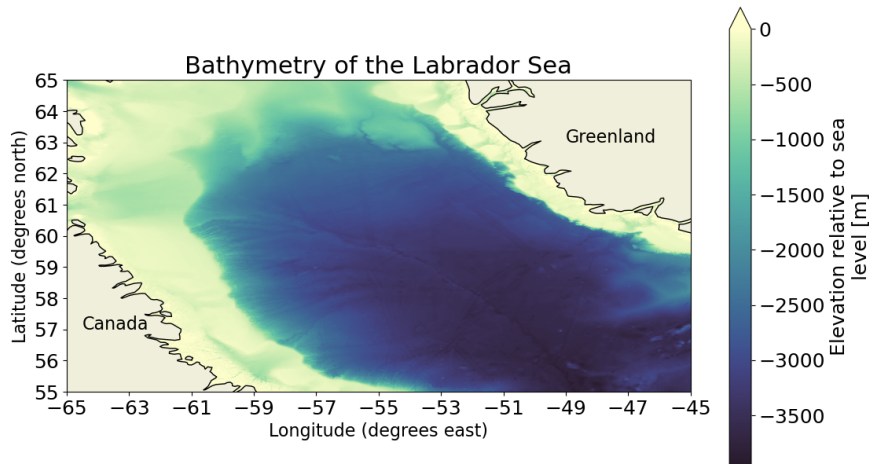


Figure 13: The bathymetry of the Labrador Sea, the data are from GEBCO Bathymetric Compilation Group (2020)

The bathymetry of the Labrador Sea is shown in figure 13. As can be seen in the figure, the Sea is almost totally enclosed by a continental shelf on all sides but the southwest. In winter the sea is partly covered with sea ice, mainly on the northern and western side, on the continental shelf. In the interior of the sea the bathymetry reaches depths of about 3500 meter. The tidal currents are dominated by a semidiurnal tide with the strongest currents in the shallow parts of the sea in the west and northeast (figure 14).

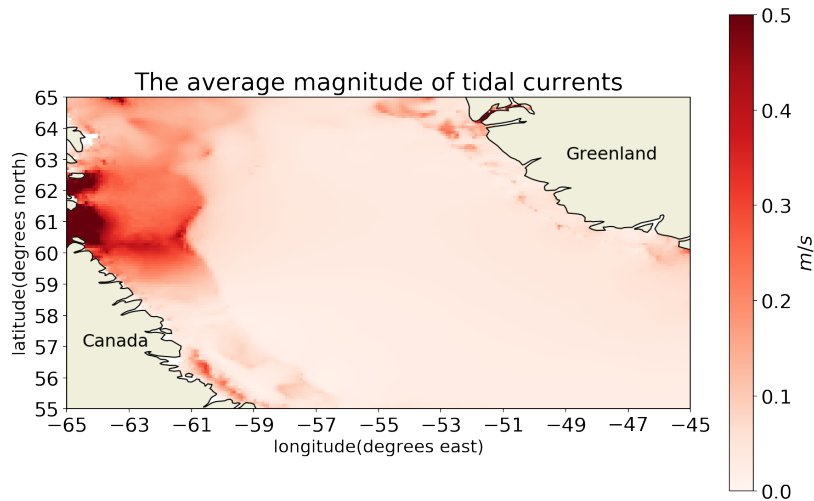


Figure 14: The time averaged magnitude of the tidal currents. The data are from the SMOC project of CMEMS, which uses tidal data from the FES2014 tidal model. This model includes the 34 largest tidal components. The currents shown in this figure are dominantly generated by the M2 tidal component.

In the Labrador Sea we can divide mesoscale eddies into three different categories: Irminger Rings, convective eddies and boundary current eddies (Rieck et al., 2019). Irminger Rings are usually anticyclonic eddies with a diameter of about 30-60 km. They originate in the West Greenland Current (WGC), near the coast of Greenland between 61 and 63 degrees north, from there they move westward (Rieck et al., 2019). The nature of their existence is not fully understood but studies found indications that they are produced by baroclinic instabilities, caused by the large shear gradient in that region. Convective eddies are found more in the interior, deeper regions of the Labrador Sea. They have diameters of about 20-30 km and they

probably originate from baroclinic instabilities at rims of convective areas (Chanut et al., 2008). Boundary current eddies are generated near the boundary currents at both the Greenland coast (the WGC) and at the coast of Canada (the Labrador Current). These eddies do not travel far from the boundary currents have diameters of about 20-30 km (Chanut et al., 2008).

### 6.1.2 Drifter description and data processing

Drifter data is widely available throughout the global ocean. These drifters are floating satellite-tracked buoys that ‘drift’ with surface currents creating a global database of surface current data. A large part of these buoys are part of the Global Drifter Program (GDP) of NOAA. This program has created a continuous dataset of more than 40 years, nowadays consisting of more than 1300 buoys that send their location every 1-2 hours (Hansen and Poulain, 1996). Over the last two decades, the drifter tracking system has mostly changed from ARGOS to GPS, greatly increasing the accuracy of the location fixes from several hundreds of meters to several tens of meters (Elipot et al., 2016). The buoys have a drogue attached that extends from about eight to fifteen meter depth, to reduce the effect of windage and wave transport. All drifter trajectories that were used for this study are plotted in figure 15.

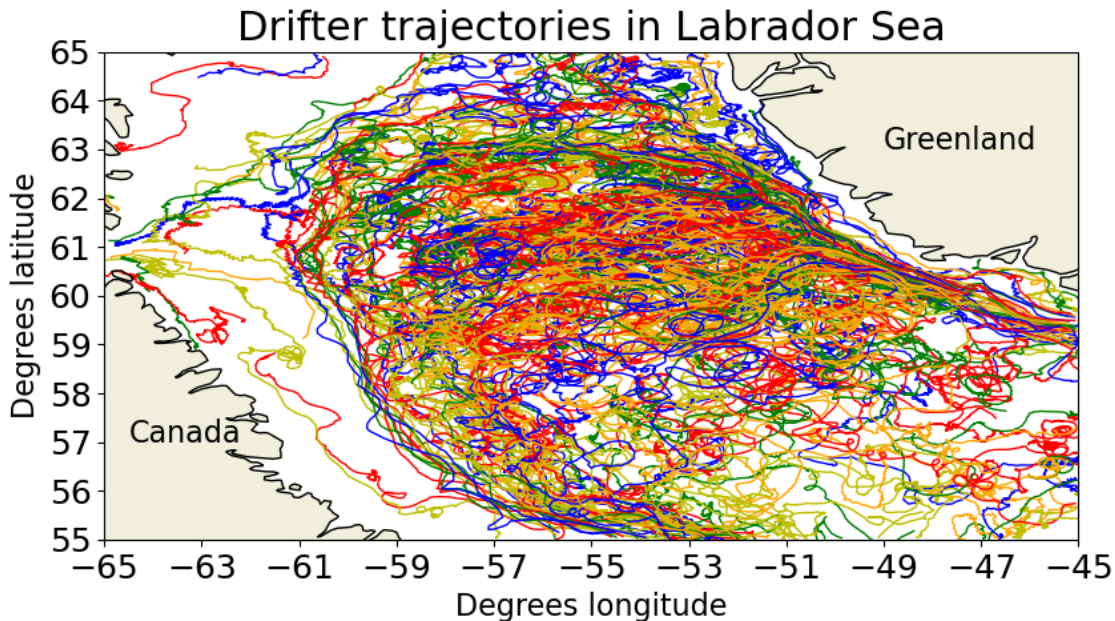


Figure 15: All drifter trajectories in the Labrador Sea used for this study

Observational data that we used, we got from the GDP of NOAA (Lumpkin and Centurioni, 2019). We limited our dataset to the domain of  $-65^{\circ}$  to  $-45^{\circ}$  longitude and  $55^{\circ}$  to  $65^{\circ}$  latitude. The data we used was already pre-processed by NOAA (Hansen and Poulain, 1996), removing outliers and interpolating the irregularly obtained data to a regular time interval of 6 hours. This interpolating was done by a process called kriging (Cressie, 1991), using the five datapoints before and after the interpolated value. Since the interval of a datafix is usually around 1-2 hours for our dataset, the interpolation period is approximately 10-20 hours. For further information about the processing of NOAA we refer to Hansen and Poulain (1996) and for information about kriging to Cressie (1991). NOAA also calculated the velocities at this same time interval by taking central differences (Elipot et al., 2016). We further reduced the dataset by only using the drifters that use the GPS-tracking system and not the ARGOS system, to obtain better accuracy. This results in a dataset that extends from June 2012 till June 2020. Most of the data was obtained in 2019 and 2020, since a large drifter experiment was performed in The Labrador Sea in these years by Goszczko et al. (2021). They released in total 150 drifters in front of the coast of Greenland, divided over three moments, in December 2019, March 2020 and August 2020. The data that we used was filtered on whether a drogue was attached or not, we only used data where the drogue was attached, since the effect of windage and wave interaction might have an influence on the trajectory of the drifters therefore also affecting the calculated diffusivities.

The described processing resulted in a data set of 211 drifters with in total more than 80.000 datapoints, where every datapoint has location and velocity data. These datapoints were checked visually whether the trajectories were realistic, e.g. were not on land. For the statistics and for calculating the diffusivity we divided all drifters into rectangular bins of 0.25 degrees latitude x 0.5 degrees longitude. We chose this binsize because it was a good compromise between still having enough observations within one bin (for most bins on the order of hundreds to thousands) and being able to visualize enough spatial variation.

### 6.1.3 Visser method for calculating the diffusivities

To obtain the diffusivities of the Labrador Sea, we implemented multiple methods. The first method is based on a study by Visser (2008). Visser (2008) studied the spreading of plankton in the ocean. The trajectories of the plankton are assumed to be a random walk and thus the spreading of the plankton can be described as a diffusive process. The method is a bit different then previous studies in a sense that it does not calculate the correlation time scale, or integral time scale, by integrating the autocorrelations of the velocities. Instead, the angles of the different segments in the trajectories are used to calculate the correlation times scales. The idea here is that the bigger the angle is between consecutive segments of the trajectories, the faster the velocity decorrelates. We can use the same methods for our drifter data, as described in the following section. If we assume that our drifter trajectories can be described by a random walk, then the diffusivity can be characterized by the following equation:

$$k_{visser} = \frac{1}{n} s'^2 \tau, \quad (17)$$

here  $k_{visser}$  is the absolute diffusivity as calculated by the method of Visser (2008), which we will call the ‘Visser diffusivity’.  $n$  is the number of dimensions (2 in our case),  $s'$  is the residual speed (equation (18)) and  $\tau$  is the correlation time scale i.e. the time in which the velocity of the drifter becomes totally decorrelated. With residual, we mean the deviation from the mean. The residual speed is calculated by taking the observed velocities at a datapoint as calculated by NOAA. From these velocities, the monthly mean velocity of the corresponding grid cell is subtracted. These monthly mean velocities come from the reanalysis data of CMEMS.

$$s' = \sqrt{(u_{drifter} - U_{CMEMS})^2 + (v_{drifter} - V_{CMEMS})^2}. \quad (18)$$

Where  $u_{drifter}$  and  $U_{CMEMS}$  are the measured velocity from the drifter and the monthly mean velocity in the zonal direction respectively and  $v_{drifter}$  and  $V_{CMEMS}$  are the measured drifter velocity and monthly mean velocities in the meridional direction.

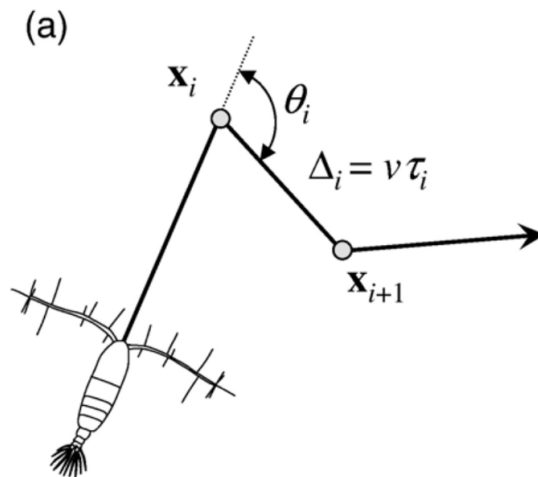


Figure 16: An illustration of a random walk, the angle between different segments of the walk is used to determine the correlation time scale (figure from Visser (2008))

The correlation time scale  $\tau$  is a measure for how long it takes before the velocity becomes totally uncorrelated. One can calculate this by integrating the autocorrelation of the velocity, however in this method we followed a different approach. For every trajectory segment, we calculated the angle it made with the zonal direction. Then for every datapoint, the difference between the angles of the segments was calculated. With this angle we calculated the correlation time scale.

$$\begin{aligned}
\langle \hat{\vartheta}(t) \cdot \hat{\vartheta}(t + \delta) \rangle &= \langle \cos \theta_i \rangle = \psi \\
\text{and} \\
\tau &= \delta / (1 - \psi)
\end{aligned}
\tag{19}$$

Here  $\hat{\vartheta}$  is the unit vector in the direction of the segment at time  $t$ ,  $\delta$  is the timestep of the observations (6 hours),  $\theta$  is the difference in angles between consecutive datapoints and  $\langle \rangle$  indicates an ensemble averaging over a grid cell. The idea of this calculation is that the larger the angle is between consecutive datapoints, the faster the velocity gets decorrelated.

This correlation time scale can then be inserted into (17). Since we used the speed instead of the different velocity components for the calculation of the diffusivity, the result is a scalar, and thus isotropic, diffusivity.

#### 6.1.4 Davis method

A different method for calculating the diffusivity was first introduced by Davis (1991). Davis (1991) work is a generalization of the work of Taylor (1922) and they define the single-particle diffusivity as the product of the residual velocity and the residual displacement:

$$k_{jk}(\mathbf{x}, t) = - \langle v'_j(t_0 | \mathbf{x}, t_0) d'_k(t_0 - t | \mathbf{x}, t_0) \rangle. \tag{20}$$

Where  $k_{jk}(\mathbf{x}, t)$  is the diffusivity, where the  $j$  and  $k$  represent tensor elements.  $v'_j$  is the residual velocity, meaning the deviation from the mean, with  $j$  indicating the direction (0 is zonal, 1 is meridional).  $d'_k$  is the residual displacement, i.e. the deviation of the displacement caused by the mean flow. The index  $k$ , indicates the direction.

The residual velocity we calculated in a similar manner as for the ‘Visser diffusivity’. For the residual displacement we ran a simulation with the Parcels model. We assume every observation of the drifter data to be the beginning of a ‘Pseudo-track’ (figure 17).

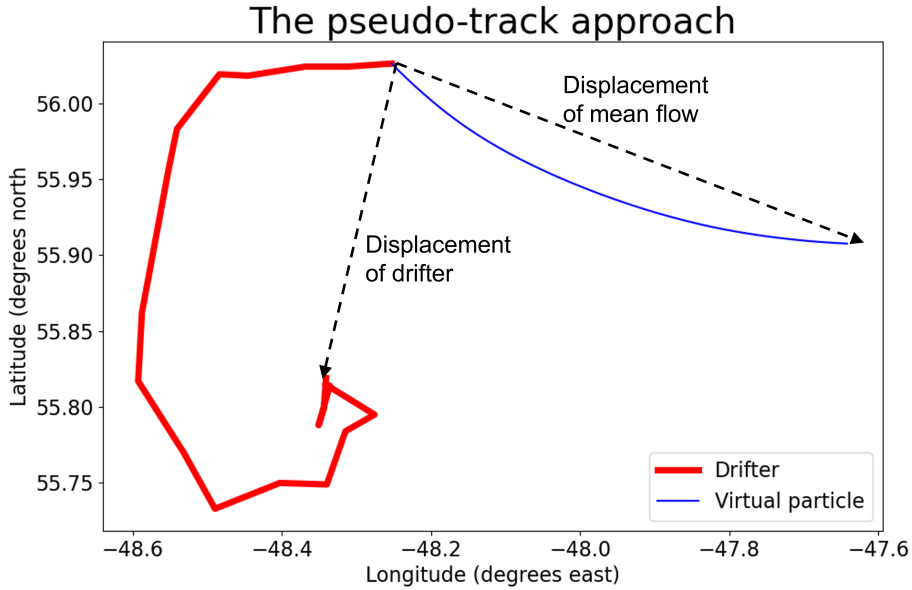


Figure 17: An example of how the displacement by the mean flow was subtracted from the observed displacement. The red line is the trajectory of a drifter in 5 days. The blue line is the trajectory of a particle that was released on the mean flow field. The displacement of the particle after 5 days was subtracted from the displacement of the drifter

For every observation, we released a virtual particle at the place and time of the observation. We simulated the displacement of this particle by running the parcels code with a monthly mean flow field that we obtained from analysis data of CMEMS. The total displacement of the virtual particle in 5 days was subtracted from the displacement of the drifter in 5 days, resulting in an approximated residual displacement. We looked at the displacement in 5 days because after an analysis of the timescales (described in section 3.7) this turned out to be the most suitable timescale. By taking an ensemble average over every grid cell, we obtained a



diffusivity tensor for every grid cell. From this tensor, we looked only at the symmetric part:

$$k_S = \frac{k_{ij} + k_{ji}}{2} \quad (21)$$

From the symmetric part, we calculate the eigenvalues and eigenvectors of the tensor for every grid cell. Now the major principal component corresponds to the largest eigenvalue and its corresponding eigenvector and the minor principal component to the smallest eigenvalue. These components indicate the major and minor directions of spreading due to diffusion. These results were plotted as ellipses on a map of the Labrador Sea.

### 6.1.5 Simulated trajectories

To be able to interpret the results of the above described calculations, we also used simulations of Lagrangian particles trapped at the surface in the Parcels framework to calculate the diffusivities. For the model the SMOC product of the CMEMS was used. The SMOC product is an hourly surface current product consisting of different components; the global circulation, the tides and stokes drift. The global circulation velocities come from the CMEMS reanalysis product; this is a global circulation model, validated with altimetry and in-situ data. It has a spatial resolution of 1/12 of a degree. The tidal velocities are generated by the FES-model (Carrere et al., 2015); A finite element solution tide model based on the barotropic tidal equations and validated with altimetry data. The stokes drift velocities come from the CMEMS wave model. In our model we only use the global circulation and the tidal components, so the results can be more easily compared to the results of the drifter data, which is little influenced by stokes drift because of the attached drogue at 8-15 meters depth. Ideally we would use the velocities of a model at 15 meter depth, however the SMOC product only consists of surface velocities, we therefore assume that these velocities are comparable. In the model, particles are released in a regular grid over the whole domain. We released 10.000 particles every week for the entire year of 2018. These particles were advected for 5 days before being deleted again. We took ensemble averages for every grid cell over the entire particle set, therefore not accounting for any seasonality, just like with the drifter data. In our model we do not take into account the influence of sea ice in the winter months, assuming that sea ice has a low influence on the surface velocities. The diffusivities were calculated with the method introduced by Davis (1991), in the same way as for the drifter data, again subtracting the mean velocity and mean displacement. The runs were done with and without the tidal components, so we could examine the influence of the tides on the diffusivity tensor.

### 6.1.6 Scale analysis

For calculating the diffusivities from Lagrangian data, a timescale has to be defined over which we calculate the displacements, the so called integral time scale. This is the time scale by which the Lagrangian velocities get decorrelated and it can be calculated by integrating the velocity autocorrelation (LaCasce, 2008):

$$T_L \equiv \int_0^{\infty} R(\tau) d\tau. \quad (22)$$

Here  $R(\tau)$  is the velocity autocorrelation and  $\tau$  is the timelag. We calculated this  $T_L$  from our velocity data from a Parcels simulation. For this Parcels simulation we released particles over the whole domain and advected these for 100 days back in time. The velocity data that we used came from SMOC where only used the Navier-Stokes component, so no tides were included. Equation (22) assumes the autocorrelation function of the velocities to decrease exponentially and to approach zero asymptotically. In theory this is true but in practice the autocorrelation oscillates and does not approach zero. This oscillation is due to eddies that have a different speed than the mean flow (Klocker et al., 2012). Furthermore the particles may drift into regions with different mixing, causing the error in the autocorrelation to increase with increasing time lag (Davis, 1991). Therefore, integrating to infinity would be impossible and the integral time scale increases with time lag. The most common solution for this is to integrate to the first zero-crossing of the autocorrelation, assuming that at that point the velocity is fully decorrelated (e.g. Freeland et al. (1975) and Lumpkin and Flament (2001)). Although this time scale coincides more with the maximum diffusivity than with the asymptotic value of the diffusivity (Griesel et al., 2010; Klocker et al., 2012), we do adopt this method as well. Furthermore, high frequency signals like inertial oscillations and tides also cause the autocorrelation to oscillate, therefore causing the autocorrelation to reach zero much faster. These signals can be filtered out by a low pass filter, like is often done in previous studies (Rühs et al., 2018; Zhurbas et al., 2014), even though we are interested in the interactions between tides and diffusion and this would filter out the tidal effect, we assume that even though tidal effects might have a large impact on the dispersion of

particles due to the interaction with non-resolved processes, it does not have a large influence on the integral time scale itself, since it is a deterministic and periodic signal.

To investigate the different time scales that are present in the velocity signal, we performed a Fourier analysis on the velocity autocorrelations of the particles. To analyse the spectral peaks in the Fourier spectrum we compare it to a theoretical red noise spectrum. Red noise is the frequency spectrum that one obtains from a random walk process as described by the following equation:

$$x_n = \alpha x_{n-1} + z_n. \quad (23)$$

Here  $\alpha$  is the lag-1 autocorrelation and  $z_n$  is a random variable assumed to be normally distributed (Torrence and Compo, 1998). This process is also called an AR1 or a first order Markov process and it results in a so called random walk. The power spectrum of such a process can be represented by (24) as shown by **gilman1963**.

$$P_{noise} = \frac{1 - \alpha^2}{1 + \alpha^2 - 2\alpha \cos(2\pi k/N)}, \quad (24)$$

here  $P_{noise}$  is the normalized power spectral density of red noise,  $f$  is the frequency and  $N$  is the total number of observations. This function was fitted to the normalized power spectral density functions of both the meridional and zonal velocities, which were calculated in the following way:

$$P_{velocity} = 2 |u_{fft}|^2 / (2\sigma^2 N), \quad (25)$$

$$u_{fft} = \sum_{n=0}^{N-1} u_n e^{-i2\pi f n/N}. \quad (26)$$

Where  $P_{velocity}$  is the normalized power spectral density,  $u_{fft}$  is the one-sided Fast Fourier Transform of the velocity autocorrelation,  $N$  is the total number of observations,  $\sigma$  is the standard deviation of the velocity and  $f$  is the frequency.

The red noise spectrum was fitted to  $P_{velocity}$  with a least-squares fit, to find the correct value for  $\alpha$ . Now, to check whether the spectral peaks that were observed are not produced by noise, we calculate a 95% confidence interval. For this we assume the velocities of the noise to be normally distributed, all Fourier components are also normally distributed (Chatfield, 1989). The squares of the Fourier components are then  $\chi^2$  distributed with two degrees of freedom (Torrence and Compo, 1998). Therefore, to calculate the 95% confidence interval of the red noise spectrum, we multiplied the red noise spectrum with the correct 95 percentile value of the  $\chi^2$ , and we still divide this value by 2 to correct for the fact that we have a one-side spectrum (**gilman1963**).

## 6.2 Results

### 6.2.1 Timescale analysis

As mentioned in the theory section, to calculate the diffusivities from the trajectories of particles, we first need a Lagrangian integral timescale. We calculated this from the autocorrelations of the velocities of the trajectories calculated by the Parcels simulation. The results are shown in figure 18. As we can see from the figure, the integral timescale ranges from about 1-5 days. Meaning that depending on the location, the velocity from the released particles gets totally decorrelated in 1-5 days. For the meridional direction this is relatively constant; around 1-2 days for the biggest part of the domain, with slightly higher values in the Northwest. For the zonal direction the values are a bit more variable, with a patch of longer timescales at the North-western coast of Greenland.

For the diffusivities we are interested in the asymptotic values, which are reached as soon as the velocity is totally decorrelated. It would be best to use the minimum value for the ITS for when this asymptotic limit is reached, since for larger timescales there can be more uncertainty in the diffusivities due to long term periodicity or other long term effects. However, out of convenience we use one value for the ITS for the entire domain. For this value we use 5 days, so we know for sure that almost all particles will be decorrelated by that time.

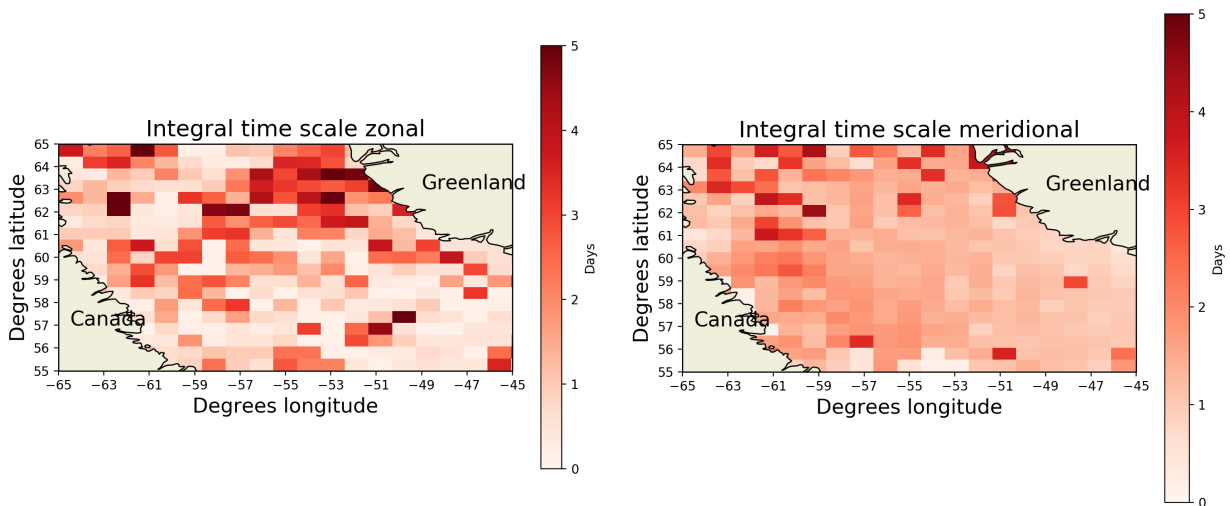


Figure 18: The integral timescale (ITS) for the zonal (left) and meridional (right) direction. The ITS was calculated from the velocity autocorrelations from the parcels simulation.

In the figures 19 and 20 the frequency spectra of the velocities of all particles are shown. These spectra are for the run without tides. The red noise spectrum that we fitted is the spectrum that follows from the assumption that the trajectories are caused by a random walk. The green dashed line is the 95% confidence interval, meaning that all peaks above this line are likely to not be caused by a purely random walk process. For both the meridional and the zonal direction we can see that there is a sharp peak at a frequency of about 1.7 per day. This signal comes from inertial oscillations. At this latitude these oscillations have a period of about 13.8 hours, which indeed results in a frequency of 1.7 per day. For both the zonal and the meridional velocity there is another peak at about 0.3 per day, this could be the result of eddy activity, however we can not be totally certain of this. In these spectra, the tidal components were switched off. When we turned the tidal components on, there were also clear peaks at 1 per day and 2 per day (the K1 and M2 components). Also the S2 component was visible. This is logical because these components are all included in the FES tidal model, which is the source of the SMOC tidal components.

The fact that not all signals fall into the confidence interval of the red noise spectrum indicates that the trajectories can not be described by a random walk, since there are some clear deterministic peaks in the signal. For practicality we still make this assumption though.

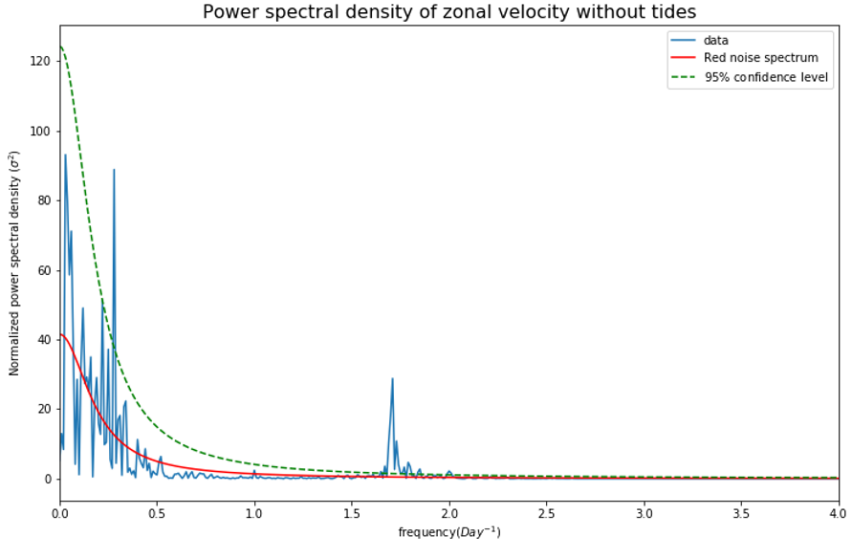


Figure 19: The frequency spectrum for the zonal velocity of the virtual particles in the Parcels simulation. The red line indicates the theoretical red noise spectrum that has been fitted to the data. The green line is the 95% confidence interval for the red noise spectrum, peaks above this line are considered significant (not caused by a random walk process).

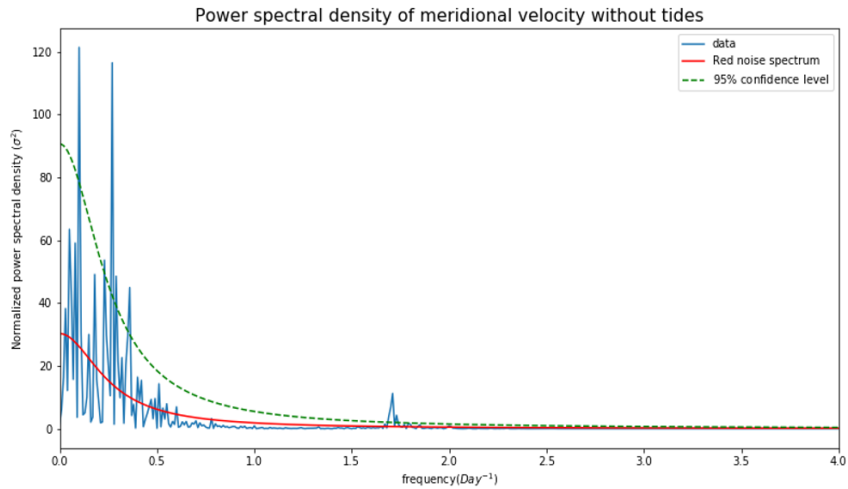


Figure 20: The frequency spectrum for the meridional velocity of the virtual particles in the Parcels simulation. The red line indicates the theoretical red noise spectrum that has been fitted to the data. The green line is the 95% confidence interval for the red noise spectrum, peaks above this line are considered significant.

### 6.2.2 Drifter observations

In figure 21 the diffusivity as calculated by the method of the Visser (2008) is shown. In the figure there are two clear distinctive regions where the diffusivity is a lot higher than in other regions; at the southwest of Greenland and along the coast of Canada, mainly in the southern part of the map. The order of magnitude ranges between a few hundred  $m^2/s$  for the deeper regions at the south-east of the basin and at the shelf at the northwest of the basin, till more then 8000 for the red regions. These regions where the diffusivities are higher coincide well with the areas where the surface currents are strong as can be seen from figure 12. Also in the north-west of the domain there is a high diffusivity calculated, the data coverage in this region is however not good so the result may not be significant.

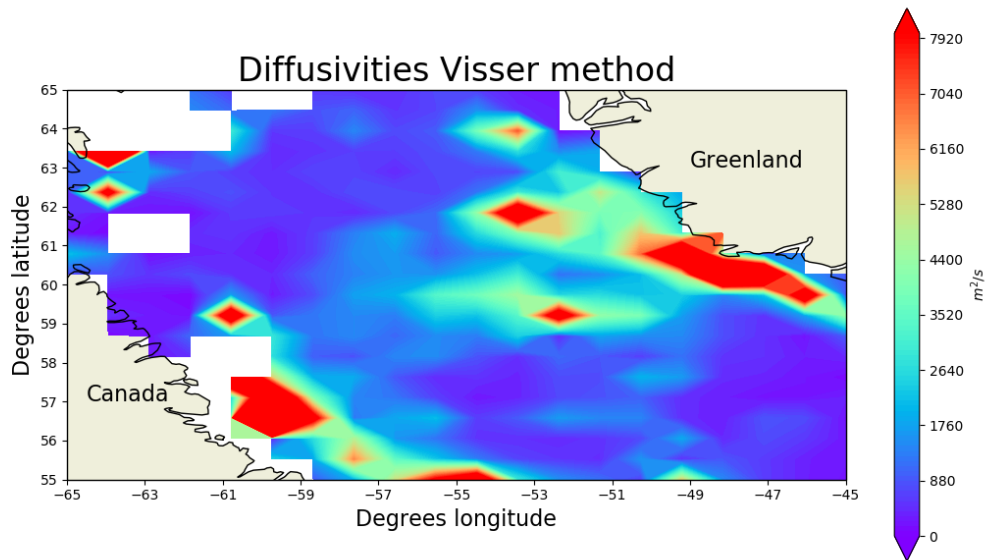


Figure 21: The diffusivities as calculated with the method of Visser (2008)

The results from the method of Davis (1991) show ellipses for the diffusivity tensors for the whole domain (figure 22). From the symmetric parts of the diffusivity tensors the major and minor principle components have been calculated. The major axis of the ellipses give the magnitude and direction of the major principle components and the minor axis gives the minor principle component. Note that a perfectly round circle would indicate an isotropic diffusivity, the more elongated the ellipse is the more anisotropic the diffusivity is. Also here there are two clear regions where the diffusivities are much higher then in the rest of the domain. From this figure it also becomes clear that in the regions where the diffusivities are higher there is often also more anisotropy in the diffusivities as can be seen from the more elongated ellipses. The magnitude of the diffusivities from the method by Davis (1991) seems to be a bit higher but still in the same order of magnitude with several hundreds of  $m^2/s$  for the lower values and up to 10000-20000  $m^2/s$  for the higher values of the major principle component. These values are however difficult to compare since we are now distinguishing between the different components in the diffusivity matrix, while in the method by Visser (2008) we assume the diffusivity to be isotropic. Another thing that stands out is that the major axis of the ellipses is often aligned with the mean currents, as shown in figure 12.

## Diffusivities calculated by the Davis(1991) method from observations

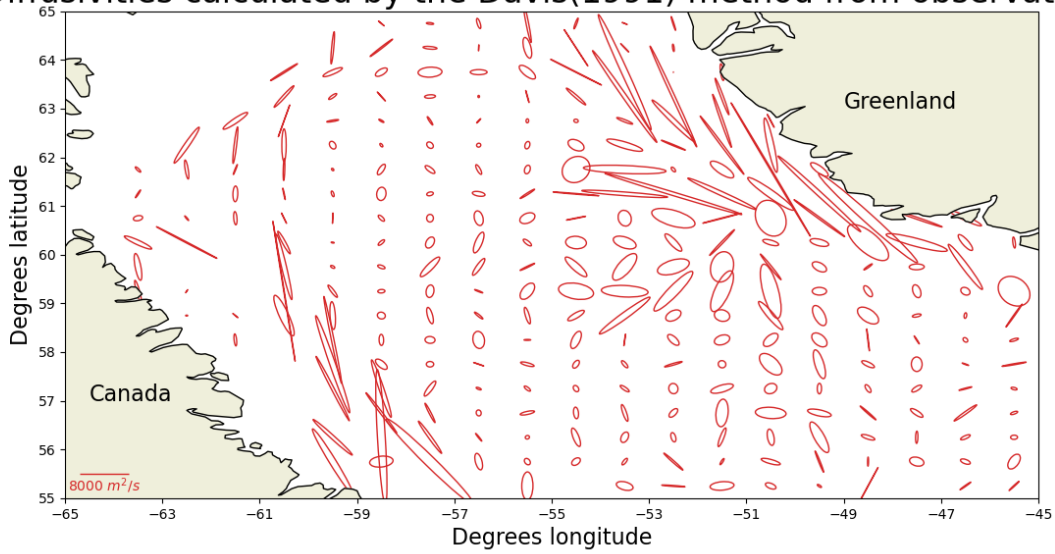


Figure 22: The anisotropy of the diffusivity tensor in the Labrador Sea. The major axis of an ellipse is the major principal component and the minor axis the minor component. Diffusivities are calculated from drifter data according to the method of Davis (1991)

### 6.2.3 Parcels simulation

The results from the simulations with the Parcels code, where virtual particles were advected on velocity fields from the SMOC product of CMEMS are shown in figure 23 and 24. The particles were advected two times with exactly the same parameters, but once with the tidal velocity field included and once without. For most of the domain, the results of the two runs are approximately the same. Only in the northwestern part of the Labrador Sea, close to the outlet towards the Hudson Strait there are high diffusivities in the run with tides, which are not at all present in the run without tides. These diffusivities in the tidal run can reach up to  $50.000 \text{ m}^2/\text{s}$  and are anisotropic, with the major axis in a more or less east-west oriented direction. The tidal currents also have this east-west orientation in this region.

In both runs we do see slightly increased diffusivities in the North Eastern part of the domain, close to the West Greenland Current and also at the southwestern part, at the Labrador Current. Note however that the scale in this figure is different from the results obtained from the drifter observations (figure 22). The values of the diffusivities from the parcels simulation, in this figure are much smaller than the ones from the observations. It does also seem that near the boundary currents, the diffusivities are slightly more anisotropic than in the interior of the domain.

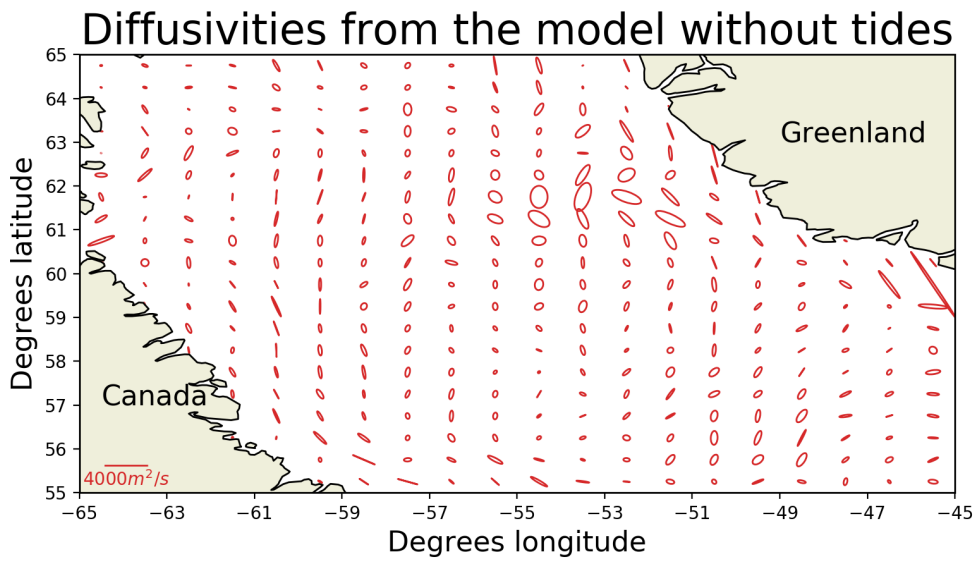


Figure 23: The anisotropy of the diffusivity tensor in the Labrador Sea. The major axis of an ellipse is the major principal component and the minor axis the minor component. Diffusivities are calculated from a parcels simulation on data from the SMOC product of CMEMS according to the method of Davis (1991). The simulation did not include tidal velocities

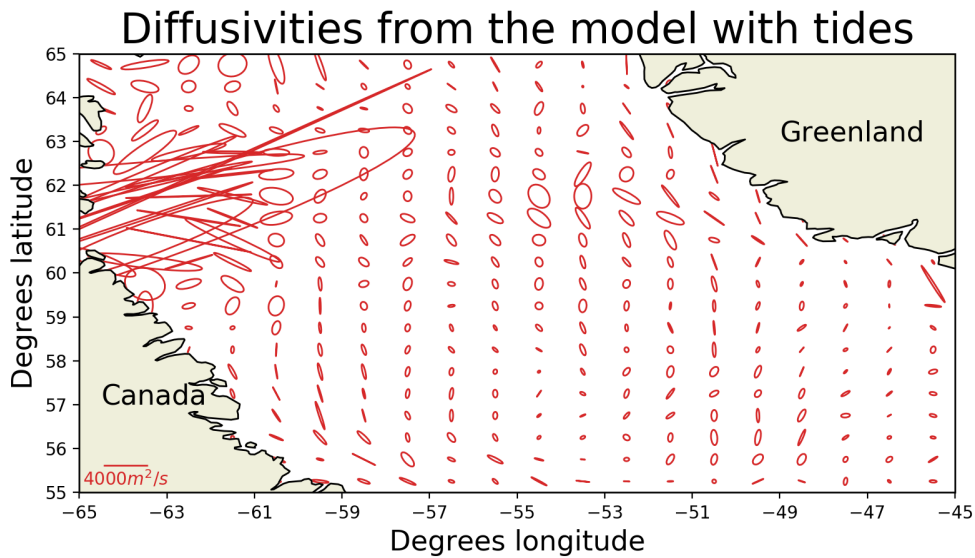


Figure 24: The anisotropy of the diffusivity tensor in the Labrador Sea. The major axis of an ellipse is the major principal component and the minor axis the minor component. Diffusivities are calculated from a parcels simulation on data from the SMOC product of CMEMS according to the method of Davis (1991). The simulation included tidal velocities

## 7 Discussion

### 7.1 Observations vs simulation

The results of the Parcels simulation do not compare very well with the results from the drifter observations. Possible explanations for this might be that something went wrong with subtracting the mean flow from the drifter observations. We subtracted the monthly averaged Eulerian means obtained from the CMEMS reanalysis data. As we have seen in the theory section, the mean flow can have a large influence on the values of the diffusivities that we calculated. The fact that we subtract a time averaged flow from the total flow, means that we differentiate the flow into different timescales, the long time scales which we regard as the 'mean flow' and the short time scales that we regard as the 'residual flow'. This assumes however that there is a clear separation between these timescales and that the eddy diffusion as we describe it only depends on the short time scales. We make the distinction between the long and the short timescales to be one month, implicitly assuming that eddies are averaged out over this timescale and that the mean flow does not vary too much in a 30 day period. These assumptions are arguable, however our time scale analysis does indicate that decorrelation time scales are on the order of 1-5 days, therefore supporting these assumptions. Another, more common, way to calculate the mean flow is by averaging the drifter velocities over time and binning them into spacial bins (Davis, 1991; Zhurbas et al., 2014; R hls et al., 2018). An advantage of this is that one does not need any Eulerian data, the calculated diffusivity is a purely Lagrangian statistic and it the mean is calculated from the same data as the total velocities. Furthermore, when using Eulerian data, the effect of sub-gridscale advection is not taken into account, a problem that is not present when using Lagrangian data (Drijfhout et al., 2003; van Sebille et al., 2018). For this to work however, one does need a substantial amount of drifter data and even then there may not be enough data available to account for temporal variability. Therefore, often long time mean (on the order of years) are taken to calculate the mean flow, thus not taking into account seasonal effects. We chose to use the Eulerian reanalysis data of CMEMS because we think that our data coverage was not good enough to calculate the means from the drifter data.

Another reason that the results of the observations and simulations do not match very well is that the amount of diffusion that we find from the model simulations depends on the grid size of the model that we use to advect the particles. We used the CMEMS reanalysis data with a spatial resolution of 1/12 degrees and a time resolution of 1 hour. This means that features that are smaller than this scale might not be totally resolved. Also, in the Parcels model, the velocity field is interpolated linearly from the CMEMS data, this can give lower shear values than in reality, it smooths out small variations in the velocity field. The interaction of this shear and smaller scale features might result into an effective diffusion that is present in the observational results, but not (or less) in the model. If this is the case, one would expect especially high diffusivities in the boundary current regions, where the shear is highest and where we expect most turbulence and eddies. This is indeed exactly what we see in the observational data and it would also explain why the diffusivities are more anisotropic in these regions, since shear dispersion only enhances the diffusivity in the along-flow direction. It is less likely that this effect is caused by the tides though, since then we would see this back in the results from the Parcels simulations that include tides. To examine whether our differences between the observations and simulations are indeed because of these non-resolved features, one could do the same study, but then with an even higher resolution. The higher the resolution of the Parcels simulations, the better it should agree with the observational data.

### 7.2 Drifters and water particles

In our study we use surface drifters as a proxy for passive tracers and for water particles. Therefore, we assume that the drifters exactly follow the flow of the water particles and can thus be used to calculate the eddy diffusivity. In fact, this assumption is not totally correct, since the drifters are stuck to the surface and can therefore only move in the horizontal. Furthermore, it assumes that there is no slippage, e.g. that there is no velocity difference between the float and the surrounding water particles. For individual floats this might not be a good approximation, however Davis (1991) showed that slippage does not have a significant influence on the Lagrangian statistics. The fact that the drifters are bound to the horizontal, gives rise to the idea that internal waves might give a bias in the velocities of the drifters, since the drifters only sample part of the orbits caused by the internal waves. Davis (1991) showed however that this effect is negligible for the large scale Lagrangian statistics. Lastly, water particles are subject to molecular diffusion, something that might cause a dispersive effect that is not caught by the dispersion of the drifters. Freeland et al. (1975) showed however that this molecular diffusion, causes dispersion rates that are orders of magnitude smaller than the once caused by larger scale features like eddies, even when shear dispersion is taken into account. We can therefore conclude that drifters are a good proxy for the movement of water particles, at least when looking at the large scale statistics.



### 7.3 Integral Time Scale

An important factor in determining the diffusivity from Lagrangian data is the Integral Time Scale (ITS). We have calculated this time scale by integrating the autocorrelation of the velocities until the first zero-crossing. By doing so, we assumed that as soon as the autocorrelation is zero, we have reached our asymptotic limit of the diffusivity. Furthermore, in calculating the ITS, we used the Parcels simulation without tides. Therefore assuming that the tides do not have an influence on the decorrelation of the velocity. We thought that this assumption was acceptable, even though this might not be totally realistic, since we saw in our kinematic model that the interaction of tides with different velocity component does actually contribute to the decorrelation of the velocity. Including the tides in our analysis of the autocorrelation would however give rise to other problems, since the oscillatory behaviour of the tides would discard our assumption that the autocorrelation is totally decorrelated at the first zero-crossing. After all, after one tidal period the autocorrelation might have crossed the x-axis twice, but that does not mean there is no correlation in the velocity anymore. Therefore we think it is better to not include the tides in our analysis of the integral time scale.

After analyzing our results, we decided to use an ITS of 5 days, for our entire domain, because we are certain that after 5 days the velocity is totally decorrelated everywhere. We took a constant ITS mainly out of practical reasons, it does however give some uncertainties. Theoretically the diffusivity reaches an asymptotic limit, thus as long as we take an ITS that is long enough we would sample the diffusivity in this limit. In reality the diffusivities do not reach a perfect asymptotic limit however, they rather oscillate due to long term effects or eddies. Therefore, using an ITS that is too long gives rise to uncertainties due to these oscillations. We think however that 5 days is an acceptable value since it is long enough for the entire domain, but still relatively small compared to previous studies (Zhurbas et al., 2014; Rühls et al., 2018). To verify whether this is a good value for the ITS, one could still test the sensitivity of the diffusivities to the ITS. If the diffusivities are sensitive to the ITS, the model could still be improved by varying the ITS over the domain.

### 7.4 Seasonality and interannual variability

In our methods to calculate the diffusivities, we binned all obtained diffusivities into spatial bins. For calculating these diffusivities we subtracted the monthly mean currents. Variability in the mean currents was thus accounted for, because we always subtracted the monthly mean velocity from the corresponding month of the data. From the resulting residual velocities we calculated the diffusivities, which we then averaged over the entire time length of the experiments (2012-2020). Any seasonality or variability in the residual currents was therefore not taken into account. This is a doubtful assumption to make, since we could expect some seasonal variability in for example eddy activity. It would be fairly easy to take this variability into account by binning the data not only in space, but also in time, for example per season. For the Parcels simulation this would be a good way to investigate the seasonality of the diffusivity, however for the drifter observations the problem is that we probably do not have enough data to get accurate results for all the seasons. Yet, as more data becomes available in the future we think it might increase our understanding of eddy diffusion in this region to look at seasonal effects, as was already done in the Indian Ocean for example (Zhurbas et al., 2014).

### 7.5 Effect of tides

In our kinematic model we have seen that the tides can cause the dispersion to be very large if combined with an eddy field. In the Labrador Sea we see the largest tidal currents in the west, near the entrance of the Hudson Strait, at around 60 to 63 degrees north. Although most eddy activity in the Labrador Sea is more near the West Greenland Current and more south towards the Labrador Current, we might still expect some eddy activity from boundary current eddies. Furthermore, due to the topography and the interaction with the tides, smaller scale turbulence might also play a role. Therefore, one would expect the tides to affect the dispersion of particles and therefore the eddy diffusivity. This we see also very clearly in the results of the Parcels simulations: diffusivities calculated for the region with large tidal currents are up to an order of magnitude larger than in the rest of the domain, a feature that is not present in the run without tides. We thus think that this is the effect of the tides, interacting with the residual currents to create large effective diffusivities. The increased diffusivities are very anisotropic, with the major axis in the east-west direction. This is also the main direction of tidal currents, further indicating that the increased diffusivities are probably indeed the result of the process that we modeled in our kinematic model, where tides interact with residual currents.

We think that the main reason that this result is not visible in the drifter observation results is because there have been too few drifters reaching these areas, most follow a more eastward route, following the mean

currents (see figure 15). Another factor of influence might be that the northwestern part of the Labrador Sea is covered in sea ice in the winter months. This has no influence for the Parcels simulations, since there we do not take the sea ice into account, but for the drifters it obviously does as they can not reach this area in those months.

One might think that the effects of the tides can be clouded because of the interpolation interval of the drifter observations, which is six hours. This is not likely to influence the dispersion due to tides however. The velocity oscillations due to the tides are indeed harder to observe, since there are only two datafixes within a tidal period. The dispersion due to the tides is however not the result of this oscillation itself, but due to its interaction with residual currents. A six hourly interval for the datafixes is therefore sufficient, because the dispersion has a longer time scale than the tidal oscillations.

To observe whether the effects of the tides are also visible in the drifter observations, drifter experiments should be performed in the outlet of the Hudson Strait (or in a different area where tidal currents are strong). One could also still investigate whether there are coastal areas with a high coverage of drifters and strong tidal currents, this is however not very likely since drifters will often follow the main currents, not entering shelf seas where tides are strong.

For the effect of tides we can conclude that theoretically they have a large influence on the dispersion of particles in coastal areas. This effect has not been observed in drifter observations but is very clearly visible in our Lagrangian model simulations. We think that for the large scale circulation this effect is very minimal, as was also suggested by Sterl et al. (2020), but for local dynamics it might be important to take the effect of tides into account. To quantify this effect and to see whether we can also observe this drifter release experiments would be necessary in areas with large tidal currents.

## 7.6 Application of kinematic model

To see what kind of dispersion patterns we could expect in the Labrador Sea we evaluated the length and velocity scales in our domain. By comparing these scales to our parameters in our kinematic model we might be able to estimate which velocity components play an important role in the dispersion in the Labrador Sea. From our data we found that residual velocities have a typical magnitude of about 0.1-0.5 m/s. In our kinematic model we simulate the residual currents as an eddy field. We can thus approximate the eddy velocities to be of this order of magnitude. In figure 14 we already saw that the maximum tidal magnitude is of the order of 0.3 m/s in the West of the basin. Assuming that the tidal velocities can be approximated by a sine-function, the amplitude of the velocity is then given by multiplying this tidal magnitude with  $0.5\pi$ , giving values of roughly 0.5 m/s. The tidal excursion is then about 2 km. From the CMEMS data we also calculated typical values for the shear, by calculating the gradient in the velocities. This resulted in values for the gradient in the order of  $10^{-4}s^{-1}$ , similar to the M2 tide and inertial frequencies. The above described typical values for the Labrador Sea would translate into the following parameters in our model:  $A_t \approx 0.5$ ,  $A_e \approx 0.5$ ,  $s \approx 10^{-4}$ .

It is hard to say anything quantitatively about the dispersion according to these parameters, however we do see that in the areas where the tidal currents are strong, they are of approximately the same magnitude as the residual current velocities. That would indicate that the diffusivity might indeed get enhanced in these areas by the interaction between the tides and residual currents. The shear gradient  $s$  is a few orders of magnitude lower than the values that we used in the kinematic model. The amount of shear dispersion and the suppression of the mixing in the cross-flow direction might therefore be lower in reality than what we have modeled in our idealized model.

We do realize that we have to be careful when applying the results of the kinematic model to reality, since the amount of dispersion does not only depend on the velocity scales, but also on the length scales of the residual currents and the orientation of the tidal current relative to the residual and shear currents. Due to the more complex geometry in the ocean, we expect there to be not just one typical length scale for for example eddies, but rather a whole spectrum of scales from small scale turbulence to mesoscale eddies. This comparison is therefore more an indication that the concepts of what we observed in the kinematic model might be applied to more realistic scenarios.

## 7.7 Outlook

The modelling that we have done with our kinematic model was very idealized. There was no realistic geometry, velocity fields were overly simplified and existed only of three components. We think that for the basic principles this was sufficient to qualitatively look at the influence of these components on the resulting diffusivities. When one wants a more realistic model however, one could also look at more complex geometries, non-stationary eddy fields or a tidal current that is not stationary. This could increase our understanding of

what is happening even more and maybe give a more robust result that gives more quantitative insights as well.

Besides this, more observational data in areas with large tidal currents would show more significant results on the diffusivities in tidal areas. Since drifters in the open ocean often mainly follow the large-scale circulation, they often do not sample the velocities in these tidal areas. Therefore, a large drifter release experiment in a tidally active area would be a great way to further investigate the above presented theories. One could use the same methods as used above, or also multiple-particle statistics, where the relative distances between drifter pairs would be used to calculate the diffusivities. More observational data also provides more opportunities to account for temporal variability by binning observations into seasons for example.

## 8 Conclusion

We have shown that for a theoretical model with a tidal flow and an eddy flowfield the tides can cause a large effective diffusivity, due to the interaction of tides with the residual flow. The size of this diffusivity depends on the amplitudes of the tidal and eddy velocities and on the tidal excursion and the eddy diameter. However, the angle that the tides make with the eddy field also influence the amount of diffusion, since the length scales are different in a different direction and the particles do not stay into one neat line of eddies. Adding a shear flow to the simulation resulted in a suppression of the mixing in the cross-flow direction. The combination of a shear flow with the tides and eddies do however cause increased shear dispersion. We can therefore conclude that in theory, tides can have a large influence on the effective diffusivity, enhancing the diffusivity in the tidal direction. In combination with shear flow, increased shear dispersion as a result of increased cross-flow dispersion due to the tides can also greatly increase the diffusivities. These processes also cause the diffusivity to be very anisotropic.

Furthermore, we have shown with parcels simulations that in the Labrador Sea the integral time scale ranges between 0.5 to 5 days, meaning that residual velocities get decorrelated in this time. Using an integral time scale of five days, we have obtained diffusivities for the entire Labrador Sea with two different methods; one introduced by Visser (2008), resulting in an isotropic diffusivity and one introduced by Davis (1991), resulting into diffusivity tensors. Both ways show qualitatively the same picture; with high diffusivities in the boundary current areas at the coast of Greenland and Canada. In the results from the method by Davis (1991) we can also see that these high values of the diffusivities tend to be more isotropic, with the major principal component often being in the direction of the mean flow. In Lagrangian simulations we used the same methods but now with virtual particles. Here these areas with high diffusivities were however much less well pronounced. In general the values for the diffusivities were lower than in the observational data. We think therefore that the increased diffusivities that we see in the areas with strong boundary currents (and thus also with larger shear) are mainly caused by small scale features and shear dispersion, which is less present in the parcels simulation, since in the Parcels model the velocities within a grid cell are interpolated linearly, therefore smoothing out small scale structures. In our theoretical model we showed that shear can cause the diffusivities to be much larger in the along-flow direction, thus supporting this conclusion.

In the theoretical kinematic model, we showed that the tides can potentially have large influences on the diffusivities, they enhance the spreading in the direction of the tidal excursion. In combination with a shear flow, this effect is suppressed, but the shear dispersion is increased, therefore causing high and anisotropic effective diffusivities. In the Parcels simulation, we do see this effect, as the tides have a very big influence on the diffusivity in the parcels model, mainly in the western part of the Labrador Sea, near the outlet of the Hudson straight. At this location the tidal currents are also strongest. In the rest of the domain the tides do not alter the results much. In the rest of the Labrador Sea the tidal currents are however also much smaller, so this might be the reason that they do not influence the diffusivities that much. In the observational data we do not see these large diffusivities in the western part of the Labrador Sea, this may however very well be due to the scarce data coverage in this area. We can therefore conclude that for the interior of the ocean the tides do not influence the diffusivities much. For areas where the tidal currents are stronger they do probably have a large influence on the diffusivities, although for our study area this could not be confirmed with observational data. Nevertheless we think that this effect might be observed when more drifter observations are present in an area with large tidal currents.

## 9 Bibliography

- Bachman, S. D., B. Fox-Kemper, and F. O. Bryan (2020). “A Diagnosis of Anisotropic Eddy Diffusion From a High-Resolution Global Ocean Model”. In: *Journal of Advances in Modeling Earth Systems* 12.2. DOI: 10.1029/2019MS001904.
- Beerens, S. P., H. Ridderinkhof, and J. T. Zimmerman (June 1994). “An analytical study of chaotic stirring in tidal areas”. In: *Chaos, Solitons and Fractals* 4.6, pp. 1011–1029. DOI: 10.1016/0960-0779(94)90136-8.
- Carrere, L., F. Lyard, M. Cancet, and A. Guillot (2015). “FES 2014, a new tidal model on the global ocean with enhanced accuracy in shallow seas and in the Arctic region”. In: *EGU general assembly conference abstracts*, p. 5481.
- Chanut, J., B. Barnier, W. Large, L. Debreu, T. Penduff, J. M. Molines, and P. Mathiot (2008). “Mesoscale eddies in the Labrador Sea and their contribution to convection and restratification”. In: *Journal of Physical Oceanography* 38.8, pp. 1617–1643.
- Chatfield, C. (June 1989). *The Analysis of Time Series: An Introduction*. 4th. New York: Chapman and Hall, p. 194. DOI: 10.2307/3619403.
- Cressie, N. (1991). *Statistics for Spatial Data*. New York: John Wiley & Sons, Ltd, p. 900.
- Csanady, G. (1973). *Turbulent Diffusion in the Environment*. Dordrecht: Reidel, pp. 1–248.
- Cushman-Roisin, B. (n.d.). “Dispersion and mixing: Shear dispersion”. In: <https://cushman.host.dartmouth.edu/courses/engs43/ShearDispersion.pdf>.
- Davis, B. E. (1982). *On relating Eulerian and Lagrangian velocity statistics : single particles in homogeneous flows*. Tech. rep., pp. 1–26.
- Davis, R. E. (1987). “Modeling eddy transport of passive tracers”. In: *Journal of Marine Research* 45.3, pp. 635–666. DOI: 10.1357/002224087788326803.
- Davis, R. E. (Jan. 1991). “Observing the general circulation with floats”. In: *Deep Sea Research Part A. Oceanographic Research Papers* 38, S531–S571. DOI: 10.1016/s0198-0149(12)80023-9.
- Delandmeter, P. and E. van Sebille (2019). “The Parcels v2.0 Lagrangian framework: new field interpolation schemes”. In: *Geoscientific Model Development Discussions* January, pp. 1–24. DOI: 10.5194/gmd-2018-339.
- Drijfhout, S., P. De Vries, K. Döös, and A. Coward (2003). “Impact of eddy-induced transport on the Lagrangian structure of the upper branch of the thermohaline circulation”. In: *Journal of physical oceanography* 33.10, pp. 2141–2155.
- Elipot, S., R. Lumpkin, R. C. Perez, J. M. Lilly, J. J. Early, and A. M. Sykulski (May 2016). “A global surface drifter data set at hourly resolution”. In: *Journal of Geophysical Research: Oceans* 121.5, pp. 2937–2966. DOI: 10.1002/2016JC011716.
- Ferrari, R. and M. Nikurashin (July 2010). “Suppression of eddy diffusivity across jets in the Southern Ocean”. In: *Journal of Physical Oceanography* 40.7, pp. 1501–1519. DOI: 10.1175/2010JP04278.1.
- Freeland, H. J., P. B. Rhines, and T. Rossby (1975). “Statistical observations of trajectories of neutrally buoyant floats in the North Atlantic”. In: *Journal of Marine Research* 33.3, pp. 383–404.
- GEBCO Bathymetric Compilation Group (2020). *GEBCO 2020 Grid*. DOI: doi:10.5285/a29c5465-b138-234d-e053-6c86abc040b9.
- Goszczko, I., E. Frajka-Williams, L. Clement, and N. P. Holliday (2021). “Wind driven Ekman transport vs eddies-ultimate fight or peaceful cooperation in the Labrador Sea?” In: *EGU General Assembly Conference Abstracts*, EGU21-13159.
- Griesel, A., S. T. Gille, J. Sprintall, J. L. McClean, J. H. Lacasce, and M. E. Maltrud (2010). “Isopycnal diffusivities in the Antarctic Circumpolar Current inferred from Lagrangian floats in an eddying model”. In: *Journal of Geophysical Research: Oceans* 115.6, pp. 1–18. DOI: 10.1029/2009JC005821.
- Griffies, S. M. (May 1998). “The Gent-McWilliams skew flux”. In: *Journal of Physical Oceanography* 28.5, pp. 831–841. DOI: 10.1175/1520-0485(1998)028<0831:TGMSF>2.0.CO;2.

- Hansen, D. V. and P. M. Poulain (1996). “Quality control and interpolations of WOCE-TOGA drifter data”. In: *Journal of Atmospheric and Oceanic Technology* 13.4, pp. 900–909. DOI: 10.1175/1520-0426(1996)013<0900:QCAIOW>2.0.CO;2.
- Jakobsen, P. K. (Aug. 2003). “Near-surface circulation in the northern North Atlantic as inferred from Lagrangian drifters: Variability from the mesoscale to interannual”. In: *Journal of Geophysical Research* 108.C8, p. 3251. DOI: 10.1029/2002JC001554.
- Kirtman, B. P., C. Bitz, F. Bryan, W. Collins, J. Dennis, N. Hearn, J. L. Kinter, R. Loft, C. Rousset, L. Siqueira, et al. (2012). “Impact of ocean model resolution on CCSM climate simulations”. In: *Climate dynamics* 39.6, pp. 1303–1328.
- Klocker, A. and R. Abernathey (2014). “Global patterns of mesoscale eddy properties and diffusivities”. In: *Journal of Physical Oceanography* 44.3, pp. 1030–1046. DOI: 10.1175/JPO-D-13-0159.1.
- Klocker, A., R. Ferrari, and J. H. Lacasce (2012). “Estimating suppression of eddy mixing by mean flows”. In: *Journal of Physical Oceanography* 42.9, pp. 1566–1576. DOI: 10.1175/JPO-D-11-0205.1.
- LaCasce, J. H. (2008). “Statistics from Lagrangian observations”. In: *Progress in Oceanography* 77.1, pp. 1–29. DOI: 10.1016/j.pocean.2008.02.002.
- Lumpkin, R. and L. Centurioni (2019). *Global Drifter Program quality-controlled 6-hour interpolated data from ocean surface drifting buoys*.
- Lumpkin, R. and P. Flament (2001). “Lagrangian statistics in the central North Pacific”. In: *Journal of marine systems* 29.1-4, pp. 141–155.
- Maas, L. R. (1989). “A comparison of Eulerian and Lagrangian current measurements”. In: *Deutsche Hydrographische Zeitschrift* 42.3-6, pp. 111–132. DOI: 10.1007/BF02226290.
- Meyerjürgens, J., M. Ricker, V. Schakau, T. H. Badewien, and E. V. Stanev (Aug. 2020). “Relative Dispersion of Surface Drifters in the North Sea: The Effect of Tides on Mesoscale Diffusivity”. In: *Journal of Geophysical Research: Oceans* 125.8. DOI: 10.1029/2019JC015925.
- Okubo, A. (1968). *Some remarks on the importance of the “shear effect” on the horizontal diffusion*.
- Regier, L. and H. Stommel (1979). *Float trajectories in simple kinematic flows (Lagrangian trajectories/float tracks/ocean currents)*. Tech. rep. 10, pp. 4760–4764.
- Ridderinkhof, H. and J. T. Zimmerman (1992). “Chaotic stirring in a tidal system”. In: *Science* 258.5085, pp. 1107–1111. DOI: 10.1126/science.258.5085.1107.
- Rieck, J. K., C. W. Böning, and K. Getzlaff (2019). “The nature of eddy kinetic energy in the labrador sea: Different types of mesoscale eddies, their temporal variability, and impact on deep convection”. In: *Journal of Physical Oceanography* 49.8, pp. 2075–2094. DOI: 10.1175/JPO-D-18-0243.1.
- Rühs, S., V. Zhurbas, I. M. Koszalka, J. V. Durgadoo, and A. Biastoch (2018). “Eddy diffusivity estimates from Lagrangian trajectories simulated with ocean models and surface drifter data—A case study for the greater Agulhas system”. In: *Journal of Physical Oceanography* 48.1, pp. 175–196. DOI: 10.1175/JPO-D-17-0048.1.
- Sterl, M. F., P. Delandmeter, and E. van Sebille (2020). “Influence of barotropic tidal currents on transport and accumulation of floating microplastics in the global open ocean”. In: *Journal of Geophysical Research: Oceans* 125.2, e2019JC015583.
- Taylor, G. I. (1922). “Diffusion by continuous movements”. In: *Proceedings of the London Mathematical Society* s2-20.1, pp. 196–212. DOI: 10.1112/plms/s2-20.1.196.
- (Aug. 1953). “Dispersion of soluble matter in solvent flowing slowly through a tube”. In: *Proceedings of the Royal Society of London. Series A. Mathematical and Physical Sciences* 219.1137, pp. 186–203. DOI: 10.1098/rspa.1953.0139.
- Torrence, C. and G. P. Compo (1998). “A Practical Guide to Wavelet Analysis”. In: *Bulletin of the American Meteorological Society* 79.1, pp. 61–78. DOI: 10.1175/1520-0477(1998)079<0061:APGTWA>2.0.CO;2.
- Van Sebille, E., S. M. Griffies, R. Abernathey, T. P. Adams, P. Berloff, A. Biastoch, B. Blanke, E. P. Chassignet, Y. Cheng, C. J. Cotter, E. Deleersnijder, K. Döös, H. F. Drake, S. Drijfhout, S. F. Gary, A. W. Heemink, J. Kjellsson, I. M. Koszalka, M. Lange, C. Lique, G. A. MacGilchrist, R. Marsh, C. G. Mayorga Adame, R. McAdam, F. Nencioli, C. B. Paris, M. D. Piggott, J. A. Polton, S. Rühs, S. H. Shah,

- M. D. Thomas, J. Wang, P. J. Wolfram, L. Zanna, and J. D. Zika (2018). “Lagrangian ocean analysis: Fundamentals and practices”. In: *Ocean Modelling* 121.November 2017, pp. 49–75. DOI: 10.1016/j.ocemod.2017.11.008.
- Visser, A. W. (2008). “Lagrangian modelling of plankton motion: From deceptively simple random walks to Fokker-Planck and back again”. In: *Journal of Marine Systems* 70.3-4, pp. 287–299. DOI: 10.1016/j.jmarsys.2006.07.007.
- Young, W. R., P. B. Rhines, and C. J. R. Garrett (June 1982). “Shear-Flow Dispersion, Internal Waves and Horizontal Mixing in the Ocean”. In: *Journal of Physical Oceanography* 12.6, pp. 515–527. DOI: 10.1175/1520-0485(1982)012<0515:sfdiwa>2.0.co;2.
- Zang, X. and C. Wunsch (Oct. 2001). “Spectral description of low-frequency oceanic variability”. In: *Journal of Physical Oceanography* 31.10, pp. 3073–3095. DOI: 10.1175/1520-0485(2001)031<3073:SDOLF0>2.0.CO;2.
- Zhurbas, V. (May 2003). “Lateral diffusivity and Lagrangian scales in the Pacific Ocean as derived from drifter data”. In: *Journal of Geophysical Research* 108.C5. DOI: 10.1029/2002jc001596.
- Zhurbas, V., D. Lyzhkov, and N. Kuzmina (2014). “Drifter-derived estimates of lateral eddy diffusivity in the World Ocean with emphasis on the Indian Ocean and problems of parameterisation”. In: *Deep-Sea Research Part I: Oceanographic Research Papers* 83, pp. 1–11. DOI: 10.1016/j.dsr.2013.09.001.
- Zimmerman, J. T. (1986). “The tidal whirlpool: A review of horizontal dispersion by tidal and residual currents”. In: *Netherlands Journal of Sea Research* 20.2-3, pp. 133–154. DOI: 10.1016/0077-7579(86)90037-2.